information services
gwasanaethau gwybodaeth

Chalcogen-bond driven molecular recognition at work

Nicolas Biot and Davide Bonifazi*

[∗]   Nicolas Biot and Prof. Dr. D. Bonifazi

    School of Chemistry; Cardiff University

    Park Place, CF10 3AT, Cardiff, United Kingdom.

    E-mail: BonifaziD@cardiff.ac.uk

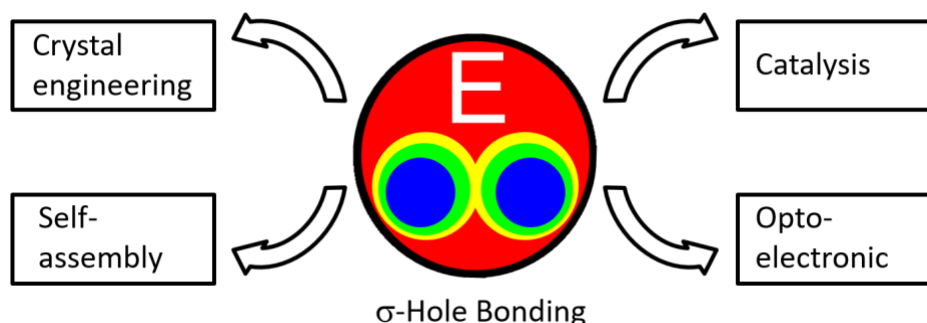**Keywords:** chalcogen bonds / tellurium / selenium / supramolecular chemistry / molecular recognition / self-assembly.

Abstract:

Out of the supramolecular toolbox, Secondary Bonding Interactions (SBIs) have attracted in the last decades the attention of the chemical community as novel non-covalent interactions of choice for a large number of chemical systems. Amongst all SBIs, halogen-bonding (XBIs) and chalcogen-bonding (EBIs) interactions are certainly the most important. However, the use of EBIs have received marginal consideration if compared to that of XBIs. By sieving the most significant examples, this review focuses on the theoretical and experimental studies carried out with EBIs in functional systems. In a systematic way the reader is guided through the most recent and representative examples in which chemists have rationally designed molecular modules that, through EBIs, trigger the initiation of chemical reactions, molecular recognition events in solutions and at the solid state to produce self-assembled and self-organised functional materials at different length scales. The study and understanding of the fundamental geometrical and physical parameters ruling EBIs is at its infancy, and it still needs to establish those principles to rationally design and program synthons that, undergoing molecular recognition through EBIs, allow the development of new tailored materials for applications in the field of optoelectronic, sensing, catalysis, and drug discovery.

Figure to the table of content.

Contents

1. Introduction.

The secondary bonding interactions (SBIs) define all interactions that "*result in interatomic contacts that are longer than covalent single bonds, but shorter than the sum of van der Waals radii*" of the atoms engaging in the contacts.[1, 2] These interactions can be extended to all close contacts involving an electron-deficient polarizable atom.[3, 4] Halogen-bonding interactions (XBIs) is certainly the most investigated ,[5-11] and its importance has been recently validated in different domains, ranging from materials to biological systems.[6, 7, 11-18] When the SBI includes electron-deficient chalcogen atoms, we refer to chalcogen-bonding interactions (EBIs, where E is a chalcogen atom; the ChBI has been also introduced recently).[19-21] In general, the contribution forces ruling an SBI are: electrostatic interactions, orbital mixing interactions and van der Waals interactions. Typically, the electrostatic contribution is described by a σ-hole, a region of positive electrostatic potential located on the X/E atom at the opposite side of the X/E-EWG bond. As far as the orbital mixing contribution is concerned, it is designated as a n_2(Y) $\rightarrow$ σ*(X/E-EWG) donation, in which the lone pair of an electro-donating atom Y interacts with an antibonding σ* orbital of a X/E-EWG bond, where X/E and EWG stand for the polarizable atom (X = halogen, and E = chalcogen) and electron withdrawing group, respectively. Descending groups XVI and XVII of the periodic table, the polarisability of the atoms increases. This is periodic behaviour is reflected in the strength of SBI, as an enhancing the positive potential of the σ-hole and a shrinking of the energy level difference between σ(X/E-EWG) and σ*(X/E-EWG) molecular orbitals is observed, thus favouring strong SBIs involving heavier elements. EBIs and XBIs are often seen as competitive interactions to hydrogen bonding interactions (HBIs), and the interested reader is addressed to the relevant papers in the field.[22-27]

Since the first observation of an EBI at the solid state in the sixties,[28] and its conceptualisation in 2000,[1, 3, 29-33] several chemical systems exploiting the chalcogen-bonding recognition

in the solid state[3, 34-37] and in solution[38] have been reported in the literature. Compared to halogens, chalcogen atoms depict two σ-holes, and can allow the formation of two interactions (*e.g.*, see the σ-holes depicted by the ESP maps of 1,2,5-telluradiazole **2Te** and iodopentafluorobenzene **1**, Figure 1).
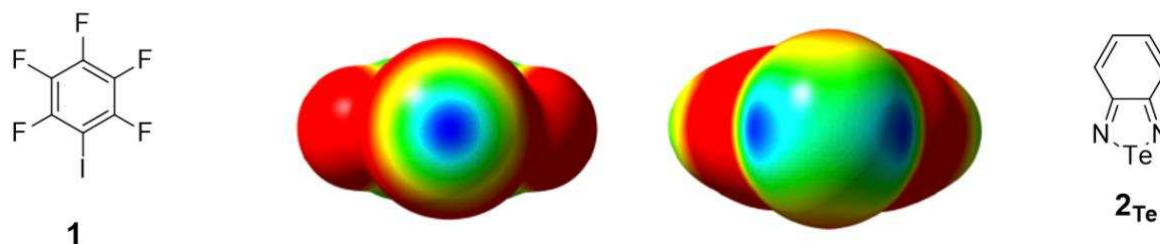
Figure 1: Iodo-pentafluoro-benzene **1** and 1,2,5-telluradiazole **2Te** and their respective ESP map (level of theory: B97D3/Def2-TZVP). The blue and the red-coloured regions correspond to the positive and negative region of the ESP map, respectively. Adapted with permission from references,[33, 38] copyright 2015 American Chemical Society.

As discussed in general terms for SBIs, three energetic contributions also pay to the strength of an EBI: electrostatic, orbital mixing and dispersion.[39] Depending on the structural motif, computational and experimental studies showed that EBIs can be dominated by electrostatic,[39] charge transfer,[40, 41] or dispersion contributions.[42] None of them should be excluded while designing molecular scaffolds establishing EBIs.[33, 43-45] Bonding models usually focus either on the electrostatic part, using Electrostatic Surface Potential (ESP) maps, or on the orbital contributions. In both cases, one can easily notice that, the more electron withdrawing is the substituent at the chalcogen atom, the stronger is the interaction, and thus the contribution of electrostatic forces. Similarly, EWGs increase the positive potential of the σ-hole and lower the energy level of the LUMO containing the σ^* orbital, thus making this orbital a better electron acceptor.[41] Having in mind these three energetic components, one can hardly fail to see that heavier atoms lead to stronger chalcogen bonds (*i.e.*, the strength of an EBI increases in the order Te > Se > S atoms). The more polarizable is the chalcogen E atom, the more anisotropically distributed is the surrounding charge, and the deeper are the σ-

holes. Taken all together this translates in a low-lying LUMO orbital and a favourable dispersion contribution.[46, 47] Building on the experimental and theoretical studies,[10, 33, 48-51] strong EBIs can be thus expected with heavier chalcogen atoms, with the Te-derived compounds establishing the most persistent and strongest interactions.[38]

While the theoretical and experimental understanding of EBIs have been extensively reviewed,[3, 45, 52, 53] here we want to focus on those examples that describe the potentialities, prospects and challenges of programming chalcogen-bonding arrays to develop new non-covalent architectures, catalysis, and functional materials.[54] Hence, in the present review, only the applications of rationally programmed arrays of EBIs will be considered to figure out the recognition modalities and the main designing principles through which one can engineer a functional EBIs-based array. In particular, the review provides an overview of the most significant examples that has impacted the field of EBIs and their practical exploitation, including catalysis, sensing, supramolecular chemistry, crystal engineering, and organic semiconductors is discerned separately in the following sections. The provided picture of the most relevant applications with EBIs can serve both as references to the exploitable aspects for engineering new materials as well as a guide to predict when an EBI can be more effective than classical non-covalent interactions to steer a function. Publications dedicated to specific EBIs-related topics can be found elsewhere, and the interested reader is addressed to the relevant reviews in the field (see below).

2. Chalcogen-bonding interactions in solution

2.1. Anion recognition

2.1.1. Anion binding involving one EBI

In solution, the use of EBIs has been mainly focused on the anion recognition.[29, 53, 55] The first example was described by *Zhao* and *Gabbaï* in 2010,[56] who reported a bidentate Lewis

acid pincer-like host, made of naphthalene derivative **3** bearing telluronium and borane functionalities (Figure 2). A binding constant of 750 M^{-1} for F^- anions was measured by UV-vis titration of receptor **3** with KF in MeOH (Figure 2b). The presence of EBIs was further confirmed by ^{19}F- and ^{125}Te-NMR spectroscopic investigations, which displayed a magnetic coupling between the ^{19}F and ^{125}Te nuclei. Titration of **3** with Cl^-, Br^-, I^-, OAc^-, NO_3^-, $H_2PO_4^-$ and HSO_4^- anions did not cause any shift in the absorption spectra, suggesting a full selectivity for the recognition of F^- anion. The study was supported by X-ray single-crystal analysis, which depicted the presence of a F^- anion at the solid state bridged between the Te and B atoms ($d_{F\ldots Te}$ = 2.506 Å, C-Te...F angle = 174° and $d_{F\ldots B}$ = 1.514 Å, Figure 2b). A similar X-ray structure was obtained for the corresponding S-analogue, although no binding to F^- anion could be detected in solution.
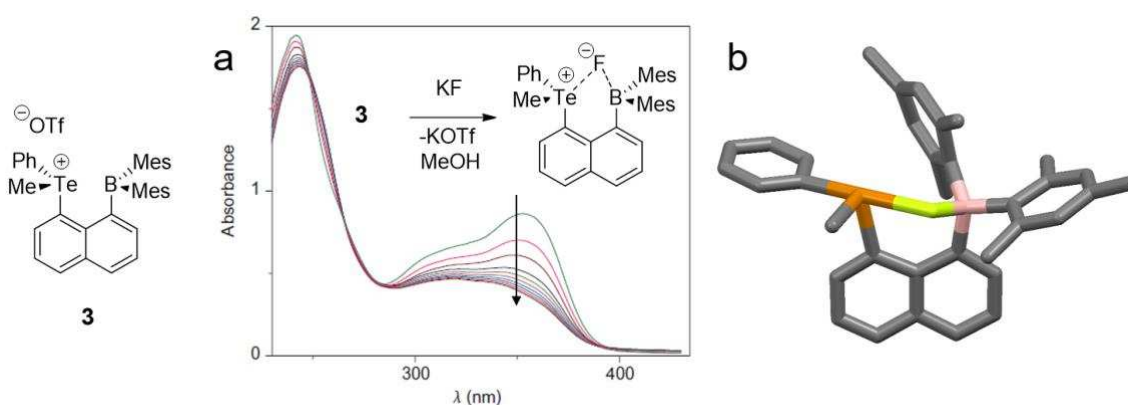
Figure 2: Naphthalene derivative **3** bearing telluronium and borane functionalities. a) UV-vis absorption spectra recorded during the titration of **3** with KF in MeOH; b) X-ray structure of the complex structure including the F^- anion. Adapted with permission from reference,[56] copyright 2010 Springer Nature.

In 2011, *Zibarev* and co-workers first published the anion binding in solution with a neutral selenadiazole.[57] In an attempt to prepare π-delocalised chalcogen-nitrogen radical anions from 3,4-dicyano-1,2,5-selenadiazole **4**, 'hypervalent' complex **5** was formed instead (Figure 3a). The strength of the EBI has been characterised in solution by steady-state UV-vis absorption titration experiments, which featured a free energy (ΔG^0_{ass}) for complex **5** of -6.6 kcal mol^{-1} and -4.7 kcal mol^{-1} in THF and MeCN, respectively. The crystal structure of complex

5 (Figure 3b) clearly depicts the short contact ($d_{S\cdots Se}$ = 2.722 Å, C-Se...S angle = 175°) between the thiophenolate and selenadiazole molecules. This study has been expanded by the same group over the years, introducing the electron deficient 3,4-dicyano-1,2,5-telluradiazole, which displays strong affinities toward halide anions both in solution and at the solid state.[58, 59]
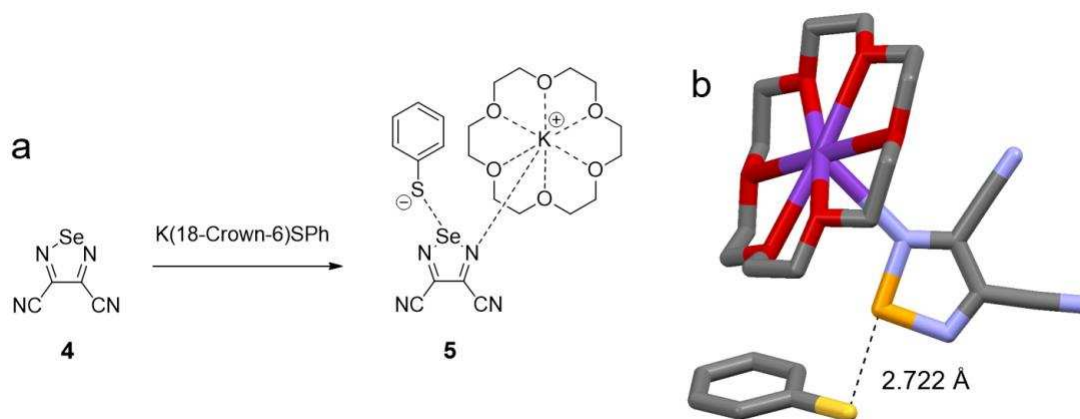
Figure 3: a) Formation of complex **5** from 3,4-dicyano-1,2,5-selenadiazole **4** upon addition of K(18-Crown-6)SPh; b) X-ray structure of complex **5**, space group: P2$_1$/n.

The first comprehensive study of an EBI-directed binding of anions in solution was reported by *Taylor*, *Seferos* and co-workers in 2015.[38] The authors described the synthesis of chalcogenadiazoles **2$_{Te}$**, **6$_R$**, **7$_E$** and **8$_E$** and their thermodynamic affinities toward different anions in organic solvents of different polarity.
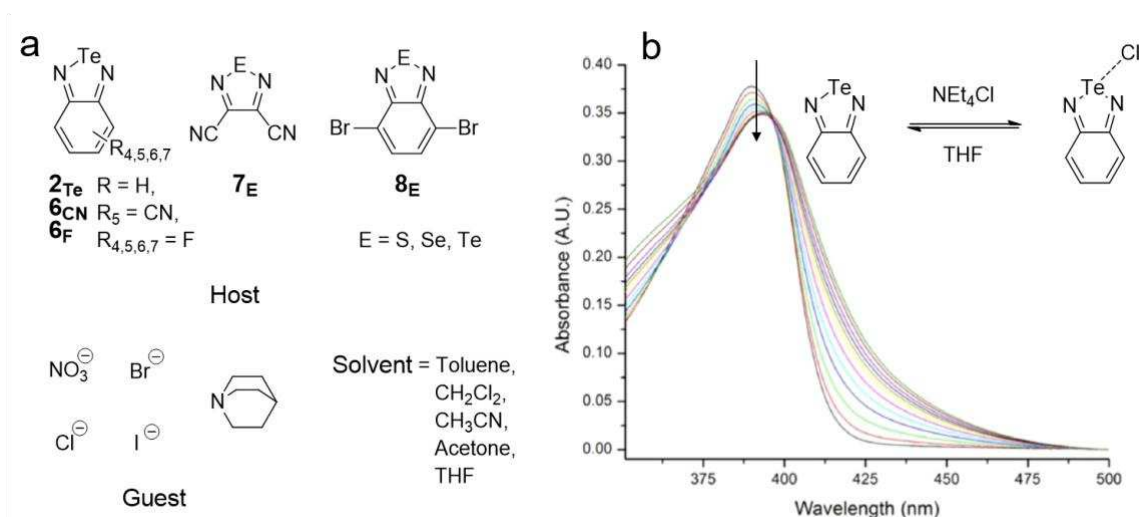
Figure 4: a) Chalcogen hosts 2Te, 6R, 7E and 8E for binding anions in solutions; b) UV-vis spectra acquired during the titration of 2Te with TBAC in THF. Adapted with permission from reference,[38] copyright 2015 American Chemical Society.

By means of steady-state UV-vis absorption titration experiments (Figure 4), K_a values up to 130 000 M-1 were measured in apolar solvents such as toluene. The experimental data revealed to be in good agreement with those obtained by DFT computational prediction performed at B97-D3/def2-TVZP level of theory, with the PCM model to account for solvent effects. The strongest EBIs have been observed for electron deficient 1,2,5-telluradiazole derivatives 3F (K_a = 130 000 M-1 and 9 800 M-1 for Cl- and Br-, respectively). Notably, a K_a value of 96 M-1 between 3F and quinuclidine was measured, suggesting that in this case the electrostatic contribution has a moderate contribution to the interaction.[38]

2.1.2. Anion binding involving two focusing EBIs: the confocal approach

Capitalising on the tellurophene motif, *Taylor*, *Seferos* and co-workers reported the recognition of anions with a bidentate host (Figure 5a).[60] Molecular pincer **10** was designed to bind anions in a pincer-like fashion, with two confocal EBIs (Figure 5b). Notably, molecule **10** displayed weaker K_a values than those measured with monodentate 6F (2 290 M-1 and 130 000 M-1 for **10** and 6F, respectively). On the other hands, reference molecule **9**, which contains only

one Te-atom, showed a low binding affinity toward Cl- (K_a = 310 M-1, *i.e.* one order of magnitude lower than that measured with **10**).
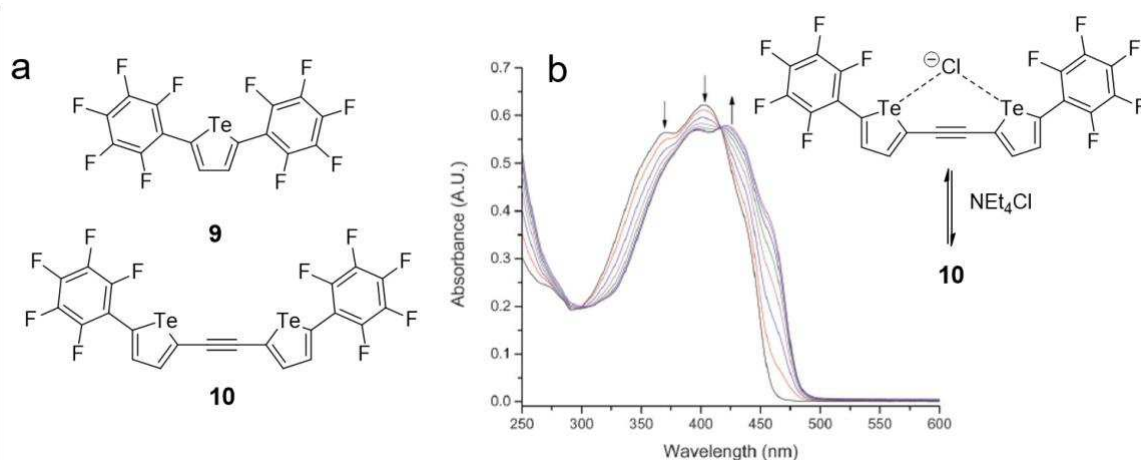
Figure 5: a) Tellurophene based chalcogen-bond donor **9** and **10** developed by *Taylor*, *Seferos a*nd co-workers; b) UV-vis spectra acquired during the titration of **10** by TBAC.[60] – Published by The Royal Society of Chemistry.

Although molecule **10** bears two chalcogen-bonding donors, at a first glance it is surprising that monodentate **6F** depicts stronger K_a values. However, if one considers that *N* atom is more electronegative than C, the Te-N bonds in telluradiazoles are significantly better acceptors than the Te-C bonds in tellurophenes. Also, given the strong directionality required by the an EBI to occur, it is hard not to see that bidentate host **10** pre-organises the EBIs along directions that are not perfectly colinear with the chalcogen donating C-Te bonds. This weakens the EBIs. Taken all together, these considerations suggest that efficient arrays of EBIs can be made if strong electron accepting chalcogen moieties are present and the geometrical constrains of the interactions are respected, namely a perfect directional alignment between the chalcogen donor and chalcogen acceptor (*i.e.*, an dihedral angle between the C-Te...X- atom of around 180°). In a parallel avenue, *Beer* and co-workers reported on the synthesis of [2]rotaxanes **11E** bearing two 5-(methylchalcogeno)-1,2,3-triazole moieties (Figure 6). Interestingly, **11Te** binds to SO42- with a K_a value of 1130 M-1 in acetone. A threefold enhancement of the strength of the association for SO42- in acetone (K_a = 3531 M-1) could be achieved with the trimethylated Se-analogues.[61] To further study the thermodynamics of the binding events, the same group

10

synthesised 5-(methylchalcogeno)-1,2,3-triazole-based molecules **12**, **13** and **14** (Figure 6) and studied their binding aptitude with different halides (Cl-, Br- and I-) in both MeCN and acetone.
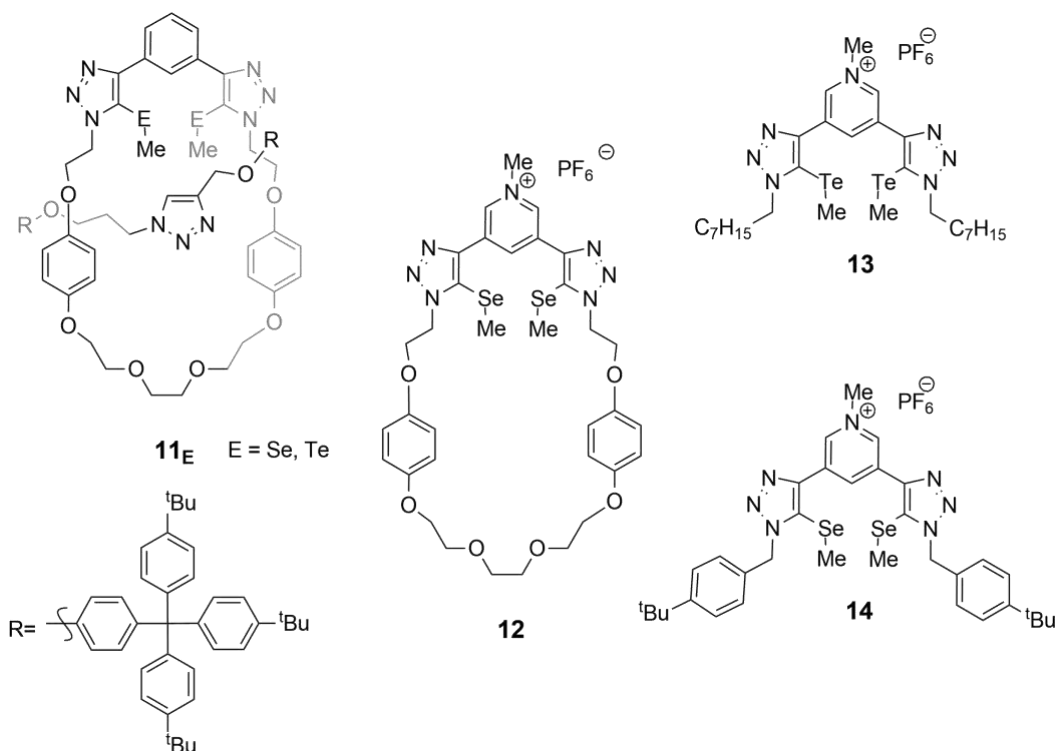
Figure 6: 5-(Methylchalcogeno)-1,2,3-triazole molecules **11E**, **12-14** studied by *Beer* and co-workers. [61, 62]

The compounds showed ΔG_{0ass} values ranging between -12.9 kJ mol-1 and -20.2 kJ mol-1, with the smallest values observed with large anions.[62] The anion binding with molecule **13** in MeCN displayed a strong enthalpic contribution, which gradually increases for large halogen anions. On the other hand, a favourable entropic contribution is only observed with Cl-, as it is negligible for Br- and unfavourable for I-. Capitalising on the 5-(methylchalcogeno)-1,2,3-triazole motif, *Beer* and co-workers also prepared foldamers bearing four halogen/chalcogen-bonding sites per unit. The molecules associate in dimeric structures developing a binding pocket motif that, featuring eight XB/EB acceptors, can strongly bind anions in water.[63] In a very recent work, the same group reported the recognition of dicarboxylate species by chiral binaphthyl-based receptors bearing HBI, XBI and EBI sites.[64] Capitalising on the geometric, steric and electronic properties of chalcogen donor functionalities, the authors demonstrated for the first time the contrasting abilities of the hosts to discriminate between stereo- (*e.g.*,

glutamate and tartrate) and geometric (*e.g.*, phthtalic and isophthalic acids) dicarboxylate isomers.[64] In addition, each receptor displays peculiar emissive sensory responses to different dicarboxylate regioisomers, further emphasizing the potentialities of EBIs in anion sensing.

Capitalising on the confocal approach, *Matile* and co-workers first conceptualised an EBI-driven approach for transporting anions across membranes (Figures 7b-c).[65] The group engineered molecule **15**, which bears a bithiophene unit functionalised with sulfone and nitrile EWGs (Figure 7a). Complex **15**•Cl- showed a dissociation constant (K_D) value of 1.13 mM. When embedded into large unilamellar vesicles, carrier **15** transported Cl- anions across the membrane with an efficiency (EC_{50}) of 1.9 µM (the transport efficiency is measured as the concentration required to reach 50% of the maximal activity). Capitalising on these results, the group also synthesised molecule **16** (Figure 7d), which featured an EC_{50} value of 0.28 µM, one order of magnitude lower than that of observed with **16**.[66, 67] In a very recent work, the Matile's group also described pnictogen bonding interactions for the anion transport.[68]
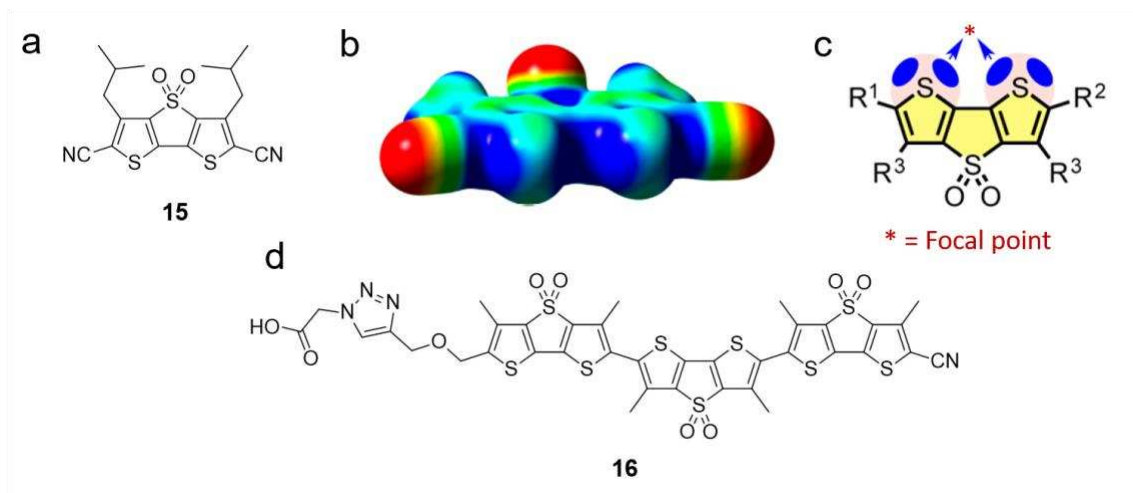
Figure 7: Chalcogen-bonding anion transporter **15** developed by *Matile* and co-workers; b) ESP map of molecule **15**, level of theory: M062X/6-311G**; c) schematic representation of the confocal approach; b) Anion transporter **16** featuring multi EBI recognition sites.[66] Adapted with permission from reference,[65] copyright 2016 American Chemical society.

2.2. Chalcogen-bonding interactions in catalysis

Considering that a number of reviews recently appeared in the literature describing the use of EBIs in catalysis,[55] this section will mainly deal with the seminal reports in the field and the key examples recently appeared in the literature. For the earlier examples and a comprehensive view of the topic, the reader is addressed to recent papers.[54, 55, 69]

2.2.1. Hydrogenation transfer reactions

Capitalising on the success of anion recognition and transport of dithienothiophene derivative **15** and of its derivatives, the group of *Matile* put forward the idea for which these compounds could also act as springboards for engineering organocatalysts (Figure 8).[70a-b] For instance, considering that the computed binding free-energy for the association of pyridine to **15** (Figure 8a) revealed to be as strong as -8.1 kcal mol-1 (level of theory: M062X/6-311G**), the group conjectured that derivative **15** could serve as a catalyst for hydrogenating quinolines.

Figure 8: a) Optimised geometry of the complex between pyridine and **15** (Me in place of *i*-Bu); dithienothiophenyl **16** b) and benzodiselenazole **18** c) catalysts; d) catalysed reduction of quinoline and e) imine.[70a-b] Adapted with permission from reference,[70a] copyright 2017 Willey-VCH Verlag GmbH & Co. KGaA, Weinheim.

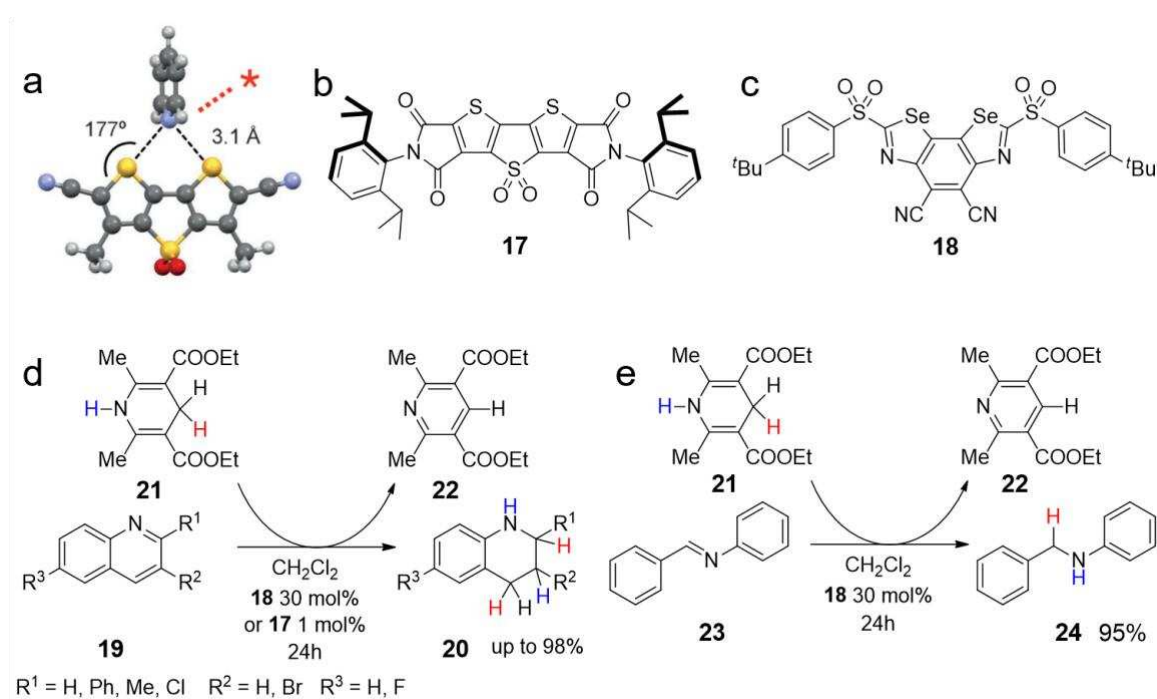It is with this idea in mind, that the group prepared different dithienothiophenyl derivatives and studied their catalytic activities. Among all substrates, compound **17** (Figure 8b) depicted the highest rate enhancement for the reduction of quinolines and imines (k_{cat}/k_{uncat} = 1 290 and 335, respectively, Figures 8d-e).[70a] In a subsequent study, the same group developed strong chalcogen-bond donor benzodiselenazoles **18**, anticipating a further kinetic enhancement of the reduction reaction. Studies showed that molecule **18** uplifted the reaction speed of several orders of magnitude (k_{cat}/k_{uncat} = 1.5 10^5) compared to that observed with **17**.[70b]

2.2.2. Reactions involving a halide abstraction

In 2017, *Huber* and co-workers reported the first catalytic halide abstraction by Se-based chalcogen-bond donors.[71] The structure of the catalysts (*i.e.*, **25** and **26**) is constituted by bis(benzimidazolium) moieties that expose alkyl selenides as the binding units (Figure 9). When two equivalents of **25SeiPr** in *d₃*-MeCN were added to a solution of **26**, amide **27** was obtained in 45% yield over 140 h.[71a] On the other hands, when chloro-compound **28b** is reacted with **28a** at -78°C in the presence of catalyst **25TeMe** in 10 mol%, product **29** is obtained in 92% over a period of 118 h.[71b] No transformations were observed in the absence of the catalysts. However, the reaction rates of these transformations remain somewhat inferior when compared to those obtained in the presence of the analogue catalysts bearing halogen-bond donors (*i.e.*, I atoms at the place of the alkyl selenides).[71a-b] Building on these results, the same group developed the first chemically-stable chalcogen-bearing organocatalysts **30TePh** able to trigger a nitro-*Michael* addition reaction.[71c-d] Kinetic studies revealed that, while S- and Se-bearing variants are inactive toward the reaction of indole **31a** with trans-*β*-nitrostyrene **31b**, the Te-based substrate featured an enhanced catalytic activity. In particular, the Te-catalyst showed an increase in the rate acceleration of 300 times compared to classical Lewis acidic H-bonding donor catalysts.[71c-d]
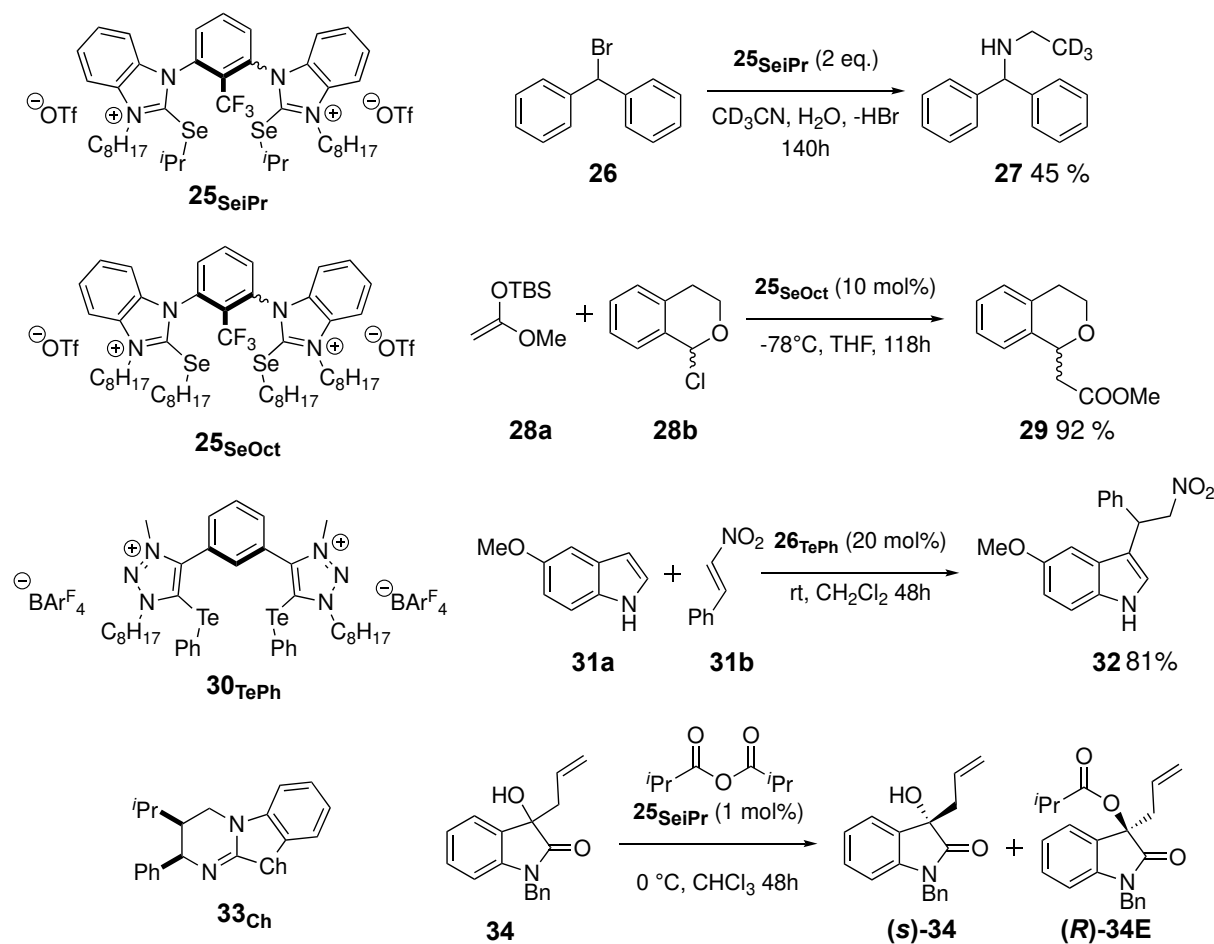
Figure 9: Catalysts used by *Huber* and co-workers in (**25Ch**) halide extraction [71a-b] and (**26Ch**) nitro-*Michael* addition[71c-d] reactions; *Smith*'s catalyst for the kinetic resolution of tertiary alcohols[72]

In a very recent work, the groups of *Willoughby*, *Cockroft*, and *Smith* systemtically studied the importance of the 1,5-O···Ch interactions in isochalcogenourea enantioselective catalysis, i.e. kinetic resolutions of tertiary alcohols, nitronate conjugate addition and formal [4+2] cycloadditions.[72] Through a combination of experimental and theoretical (DFT and natural bond orbital calculations) studies the authors showed that the N-acyl isochalcogenouronium intermediates are stabilised by EBIs interactions, with the selenium congener revealing the strongest rate enhancement and selectivity across a range of reactions. For instance, tertiary alcohol 34 could be kinetically resolved by addition of catalyst **33Te**, to give ester (**R**)-**34E** in 39% of conversion with s = 70 (er$_{ester}$ = 97:3). New works include examples in dual chalcogen−chalcogen bonding catalysis by *Wang*[73a] and reduction of quinoline by *Hantzsch* esters with chiral chalcogen-donating scaffolds by *Peluso*[73b].
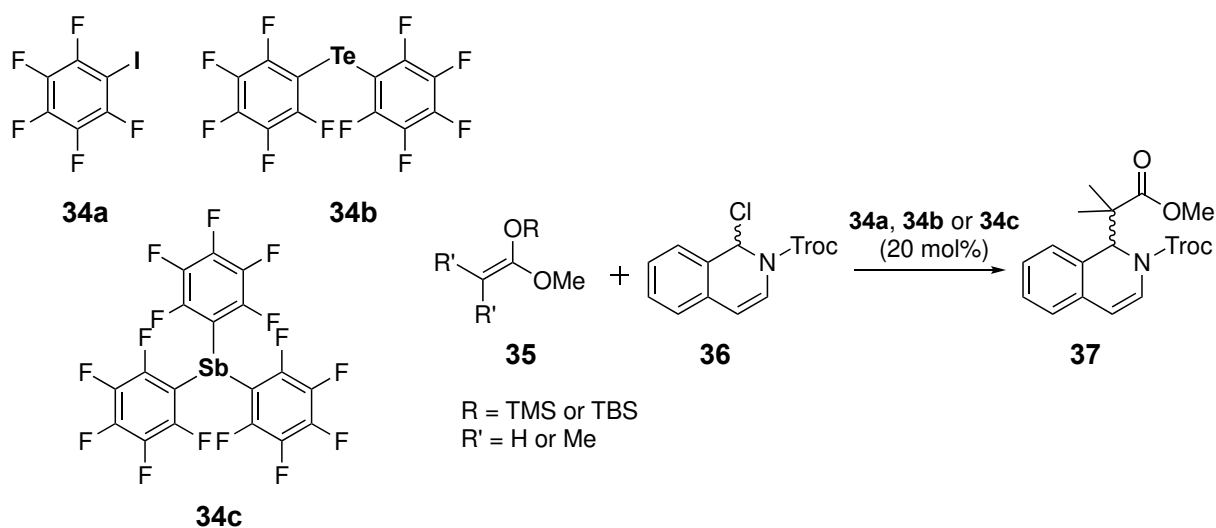
Figure 10: Catalysts **3a-c** developed by *Matile* and co-workers for the chloride abstraction reaction.[74]

In a similar chloride abstraction reaction, *Matile* and co-workers compared halogen-, chalcogen- and pnictogen-bonding catalysts (Figure 10).[74] For this porpoise, the group synthesised molecules **34a-c**, bearing the heavy-atom centre connected to pentafluorophenyl moieties, and used as catalysts in the addition reaction of enolate **35** to quinoline **36** (treated with Troc chloride). Whereas both I- and Te-bearing derivatives increased the reaction rate of 50-fold (k_{cat}/k_{uncat} = 50 and 52, respectively), Sb-doped analogue **34b** surprisingly boosted the kinetic of three orders of magnitude (k_{cat}/k_{uncat} = 4090).[74]

2.2.3. Ring formation

Very recently, *Wang* and co-workers reported on an unprecedented seven-membered cyclisation reaction triggered by chalcogen-bonding organocatalysis (Figure 11).[75] For instance, catalyst **38** was used to activate β-ketoaldehyles that, in the presence of the relevant indole, undergo cyclisation reaction to give seven-membered *N*-heterocycle **41** (Figure 11). The cyclisation reaction proceeds through sequential EBI-enabled additions, followed by a final dehydration reaction. When catalyst **42** is added to a solution of tricyclic compound **43**, a further cyclisation occurs, yielding tetracyclic derivative **44** (Figure 11). In the last transformation,

16

catalyst **42** interact with a methyl ketone of **43** to form an enol that, undergoing addition reaction to a conjugated double bound, give a bridged seven-membered N-heterocycle.[75]
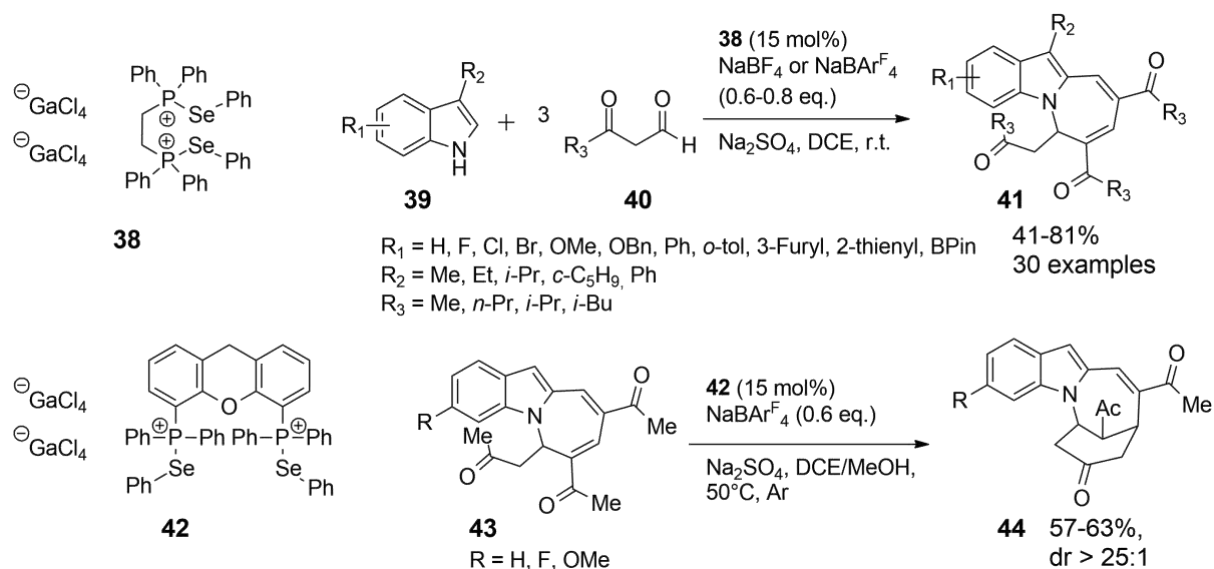
Figure 11: Catalysts **38** and **42** developed by *Wang* and co-workers and used to form **41** and **44**.[75]

2.3.   Programmed self-assembly in solution

2.3.1.   Micellar structures in water

Despite the fact that EBIs could be observed in solution for anion binding and catalysis, examples of larger self-assembled structures are very scarce in the literature. It is only in 2018, that *Yan* and co-workers published the first EBI-mediated formation of a supramolecular architecture in solution (Figure 12).[76] Building on a quasi-calix[4]chalcogenadiazole **45E** as multi-site EB-donor and on *N*-oxide-pyridine **46** as EB-acceptor, the authors reported the first preparation of a supra-amphiphile (**45E•46**) triggered by EBIs. Supramolecule **45E•46** spontaneously undergoes self-organisation in an aqueous solution, yielding different architectures depending on the strength of the EBI in play (*i.e.*, on the chalcogen atom).
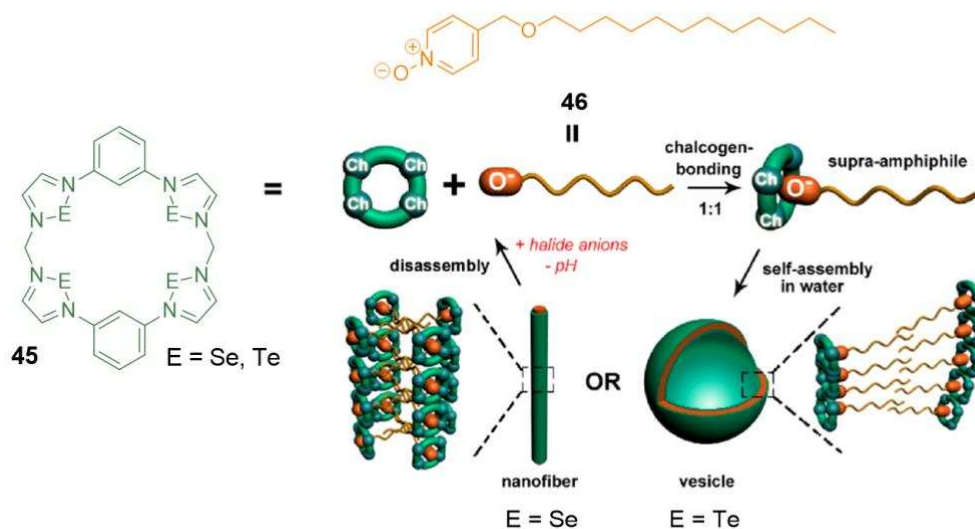
Figure 12: Quasi-calix[4]chalcogenadiazole **45E** and surfactant **46** developed by Yan and co-workers to build chalcogen-bonded nanofibers and vesicles. Reproduced with permission from reference,[76] copyright 2018 American Chemical Society.

For instance, complex **45Se•46** gives rise to nanofibers with a uniform radial diameter of 6.5 nm. On the other hand, Te-doped non-covalent analogue **45Te•46** forms spherical micelles with a critical micellar concentration (CMC) of 3.4 µM. Transmission electron microscopy (TEM) imaging showed micelles size ranging from 40 to 130 nm, with a membrane thickness of 5.9 nm as estimated by SAXS measurements.[76] The presence of an EBI within complex **45Se•46** was further characterised by UV-vis, NMR, mass spectroscopy and isothermal titration calorimetry (ITC). In particular, ITC experiments revealed association strengths of around 7.2 10_5 M$_{-1}$ and 1.4 10_5 M$_{-1}$ for complexes **45Te•46** and **45Se•46**, respectively.[76] Exploiting the reversibility of EBIs, the spherical micelles could be disassembled by addition of halide anions (Cl$_-$ or Br$_-$) or by decreasing the pH.

2.3.2. Supramolecular capsules

In a very recent paper, *Diederich* and co-workers have reported the only example to date of a chalcogen-bonded molecular capsule.[77] The structure is constituted by two resorcin[4]arene cavitands that, exposing benzotelluradiazoles walls, slowly dimerise in solution through the

development of 16 EBIs (Figure 13a). The structure has been characterised in the solid-state by X-ray diffraction analysis and in solution by NMR.
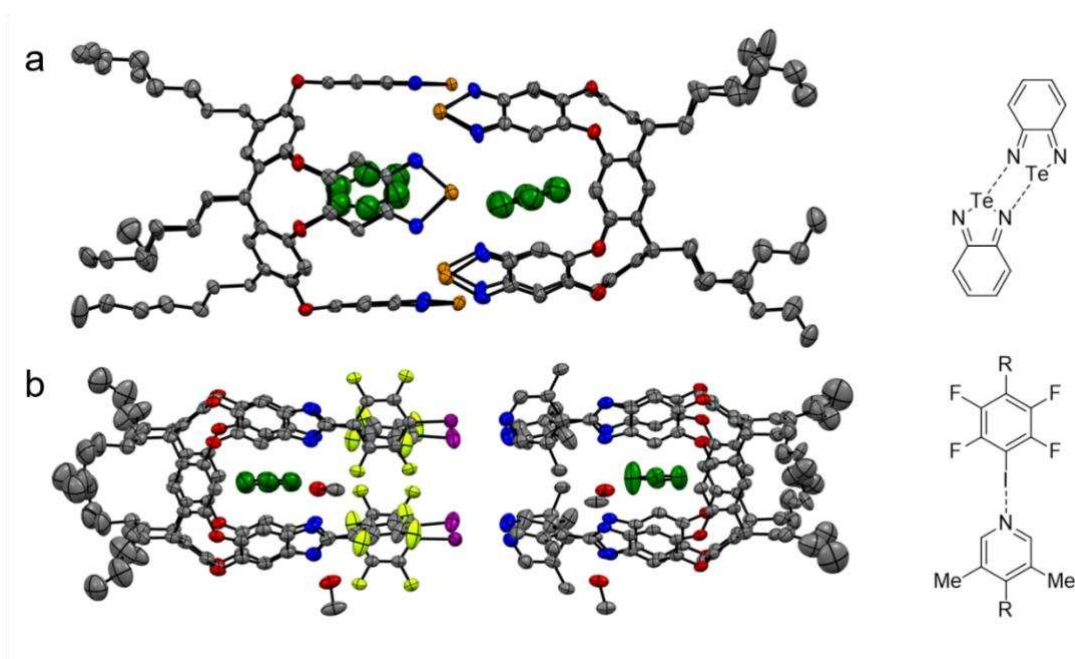
Figure 13: ORTEP representation of the X-ray structures of a) chalcogen- and b) halogen-bonded capsules reported by *Diederich* and coworkers.[77, 79] H-atoms are omitted for clarity. Space group: C2/c (a) and P2$_1$/c (b).

Quantitative electrospray ionisation mass analysis allowed the determination of the association strength, which revealed to be as high as 2.9 10$_7$ M$_{-1}$. To the best of our knowledge, this is the strongest association constant measured so far for a chalcogen-bonded non-covalent architecture. The X-ray crystal structure (Figure 13a) shows that the two cavitand hemispheres are held together by an equatorial belt-type network of short chalcogen bonds ($d_{N...Te}$ = 2.6 – 2.9 Å). Notably, two benzene molecules are trapped inside the capsule. The reference S-analogue also been also synthesised and studied. As expected, the molecule undergoes formation of the capsule with weak dimerisation association (K_d = 786 M$_{-1}$). In contrast to the persistent capsular self-assembly of the Te-bearing cavitands, the solid-state arrangement for the S-doped derivative revealed to be solvent-dependent, and two different supramolecular structures were obtained. In apolar solvents, *i.e.* benzene and toluene, a shifted capsule featuring twelve long-range EBIs ($d_{N...S}$ = 3.0 – 3.5 Å) was obtained. On the other hands, when

crystallised from CH_2Cl_2, the S-bearing cavitands arrange in an 1D supramolecular polymer in which each cavitand walls is interlocked into the cavity of the nearest neighbouring molecule. All molecule engages into $\pi-\pi$ stacking interactions ($d_{\pi-\pi} = 3.4$ Å).[77] When compared to supramolecular capsules mediated by four XBIs ($d_{N\cdots I} = 2.82$ Å, Figure 13b), the chalcogen-bonded complex features the strongest association constant ($K_a = 2.9\ 10^7$ M$_{-1}$ and 5 370 M$_{-1}$ as determined by $_1$H-NMR studies for the chalcogen- and halogen-bonded capsules, respectively).[78, 79]

3. Mastering soft matter at the molecular level through EBIs

Among all applications, EBIs finds its main use in the synthesis of supramolecular assemblies at the solid state. Given the strong orbital contribution, EBIs hold great promises to arrange small π-conjugated molecules into crystalline organic semiconductors that could be used as springboards for optoelectronic applications. It is with this application in mind, that in this section we focus the attention on those recognition motifs controlling the solid-state supramolecular organisation of polycyclic aromatic hydrocarbons (PAHs). As the topic of EBIs at the solid-state has been extensively reviewed, this manuscript mainly focuses on π-conjugated modules equipped with recognition motifs that has been designed to form either homo- or hetero-associating EBIs. For a comprehensive description of EBIs in crystals, the interested reader is addressed to the relevant reviews in the field.[1, 3, 67, 80]

3.1. Self-assembly of chalcogenadiazoles: infinite ribbons *vs* discrete assemblies

The masterpiece in the field is the 1,2,5-chalcogenadiazole recognition motif, and the most studied case is that of benzo-1,2,5-telluradiazole **2Te**. This molecule organises into ribbons at the solid state through the formation of double EBIs ($d_{N\cdots Te} = 2.682\text{-}2.720$ Å) forming non-covalent four-membered rings (Figure 14). In this arrangement each Te-atom engages in two bifurcated EBIs at an angle of 134°.[33, 81]
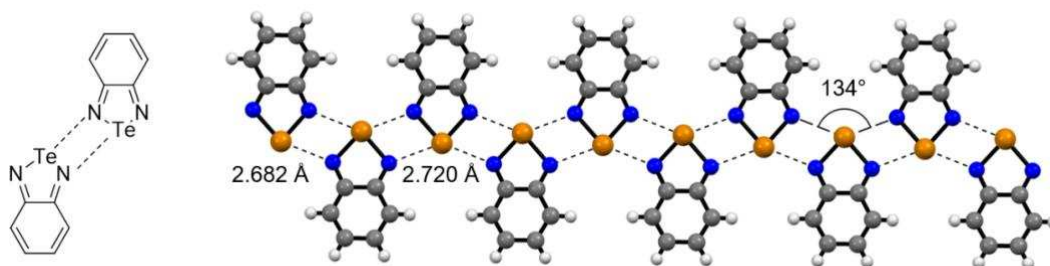
Figure 14: X-ray structure of benzo-1,2,5-telluradiazole 2_{Te} forming a ribbon-like arrangement.[81]
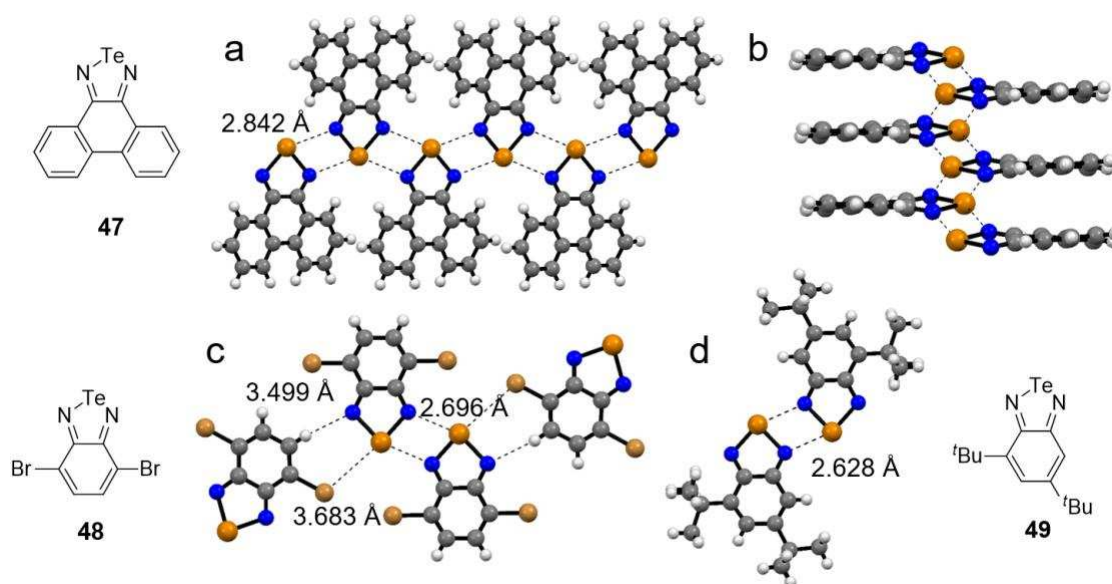
Figure 15: X-ray structure of 1,2,5-telluradiazole derivatives: a-b) top and view of **47**,[82] c) top view of **48**,[81] d) top view of **49**.[83] Space groups: P$\bar{1}$ (**47**), P2$_1$/c (**48**) and P2$_1$/n (**49**).

Lateral functionalisation of the benzo-ring leads to a loss of ribbon-like organisation, and non-infinite supramolecular structures are often formed (Figure 15). For instance, phenanthro[9,10-γ][1,2,5]telluradiazole **47** first prepared by the group of *Neidlen*,[82] undergoes formation of a polymeric structures through multiple EBIs ($d_{N\ldots Te}$ = 2.842 Å, Figure 15a). In contrast to the ribbon arrangement of benzotelluradiazole 2_{Te}, molecular units of **47** are not coplanar, rather each PAH molecule is displaced out-of-plane due to the steric hindrance exerted by the lateral benzenoid rings (Figure 15b). Notably, when passing to di-bromo derivative **48**, this molecule forms chalcogen-bonded dimers ($d_{N\ldots Te}$ = 2.696 Å) at the solid state (Figure 15c).[81] The dimers link to one another by Br...Te ($d_{Br\ldots Te}$ = 3.683 Å) and H-bonding ($d_{N\ldots C}$ = 3.499 Å)

21

interactions. Increasing the steric demand, namely through the addition of two lateral di-*tert*-butyl groups, molecule **49** solely arranges in isolated dimers through double EBIs ($d_{N\ldots Te}$ = 2.628 Å, Figure 15d).[83]
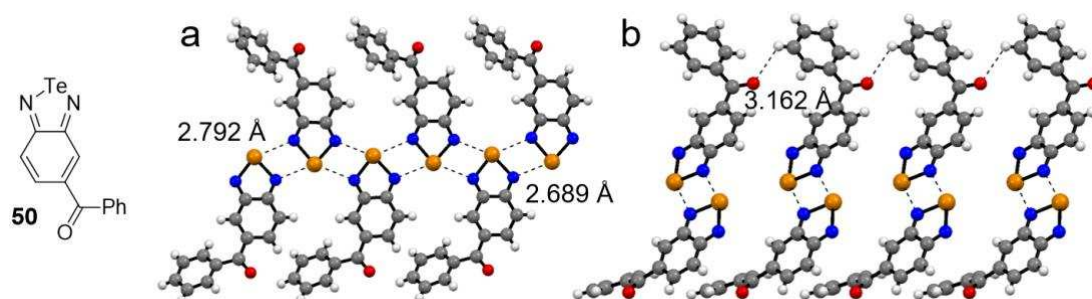
Figure 16: a) Top view; b) side view of the X-ray structure of **50**. Space group: C2.[84]

Capitalising on the benzotelluradiazole results, *Vargas-Baca* and co-workers engineered non-centrosymmetric crystals, featuring non-linear optical (NLO) response (Figure 16).[84] For instance, molecule **50** arranges into flat ribbons at the solid-state through double EBIs ($d_{N\ldots Te}$ = 2.689 – 2.792 Å, Figure 16a). Each ribbon links to one another through lateral H-bonds ($d_{O\ldots C}$ = 3.162 Å, C-H...O angle = 119°, Figure 16b). Interestingly, the crystals of both chalcogenadiazole derivatives **2Te** and **50** show static hyperpolarizability ($\langle\beta\rangle$) values of 1.60 x 10^{30} esu and 1.94 x 10^{30} esu, respectively. In particular, the $\langle\beta\rangle$ value for crystals of **50** is comparable to that of reference crystals of reference benchmark *p*-nitroaniline ($\langle\beta\rangle$ = 8.44 esu x 10^{30}) for applications in non-linear optics.[84] Although the 1,2,5-chalcogenadiazole motif depicts a strong recognition fidelity, the chemical sensitivity toward water severely limits the use this recognition unit in materials science.[85] Thus, structural congeners of the 1,2,5-chalcogenadiazole have been engineered, and derivatives bearing a 1,2,5-selenadiazole motif conceived.[86] Surprisingly, benzo-1,2,5-selenadiazole **2Se** arranges in trimeric clusters through two distinct EBIs ($d_{N\ldots Se}$ = 3.155 Å). Each cluster is connected to each other through weak H-bonds involving both N- and Se-atoms ($d_{N\ldots C}$ = 3.417 Å and $d_{Se\ldots C}$ = 3.928 Å). As no double EBIs arranged in the typical squared ring have been detected at the solid state, one can

hypothesise that in this case the Se atom is not enough polarized and electron poor to accommodate two chalcogen interactions.
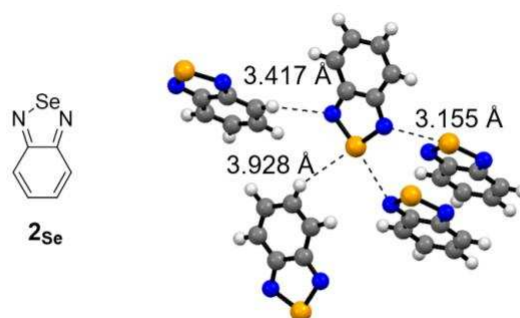
Figure 17: X-ray structure of **2Se**. Space group: Pna2$_1$.[86]

In 2014, *Zade* and co-workers reported on the synthesis of benzo-1,2,5-selenadiazole bearing different aryl moieties at the 3- and 4-positions of the benzenic substructure, *i.e.*, phenyl and thiophenyl substituents (**51** and **52**, respectively, Figure 18).[87] In these cases, both compounds **51** and **52** associates into dimers at the solid state (Figures 18a and 18b) through double EBIs ($d_N\ldots_{Se}$ = 2.993 Å and 3.424 Å, respectively). Notably, in the case of molecule **52** an intramolecular, conformationally locking, S...N interaction established between a S-atom of the lateral thiophenyl rings with the N-atom of the selenadiazole is observed. However, when selenophenyl substituents are laterally added (**53**), only intramolecular locking Se...N interactions between the N-atoms of the selenadiazole and the Se-atom of the two selenophenyl moieties are established at the solid state (Figure 18c). These EBIs force the two selenophenyl rings to adopt a *syn*-type conformation, hampering the formation of dimeric complexes.
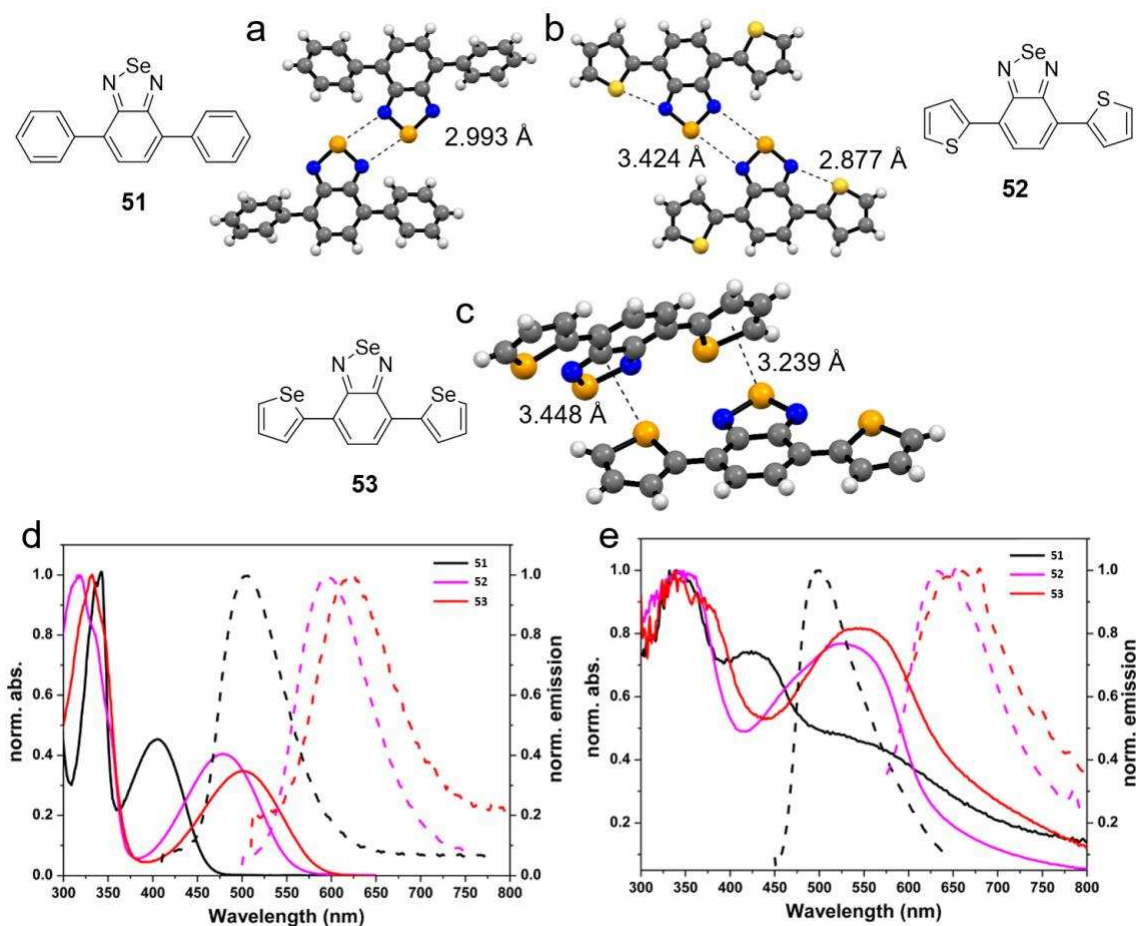
Figure 18: X-ray structure of a) **51**, b) **52** and c) **53**. Space group: P2$_1$/c (**51**), Pca2$_1$ (**52**) and P2$_1$/c (**53**). UV-vis absorption and emission profiles d) in solution and e) in thin films on ITO coated glass. Adapted with permission from reference,[87] copyright 2014 American Chemical Society.

The optoelectronic properties of selenadiazole derivatives **51**-**53** have been studied in CH$_2$Cl$_2$ by cyclic voltammetry (CV) and in benzene by UV-vis absorption and emission spectroscopies (Figure 18d). Under irradiation at 365 nm, compounds **51**, **52** and **53** emit in the green, orange and red, respectively. When deposited as thin films on ITO-coated glasses, the UV-vis absorption and emission profiles experienced bathochromic shifts and peak broadening compared to those measured in benzene solution (Figure 18e). This suggested that strong intermolecular interactions such as π-stacking are present in thin films, most likely favoured by chalcogen-chalcogen, chalcogen-nitrogen and chalcogen-π interactions.[87] Orange, yellow-green, and green emitting 4-methoxybenzene, naphthalene, and 4-nitrobenzene benzoselenadiazole-capped derivatives were also prepared,[88] and their photophysical and

solid-state assembly investigated. To strengthen the recognition fidelity of the benzo-1,2,5-selenadiazole, *i.e.* enhance the extend of the σ-hole, *Vargas-Baca* and co-workers prepared various organic crystals of **2Se** in the presence of a Bronsted acid.[89] In particular, crystals of salt **2Se•HCl** could be formed when **2Se** was exposed to HCl (Figure 19a).
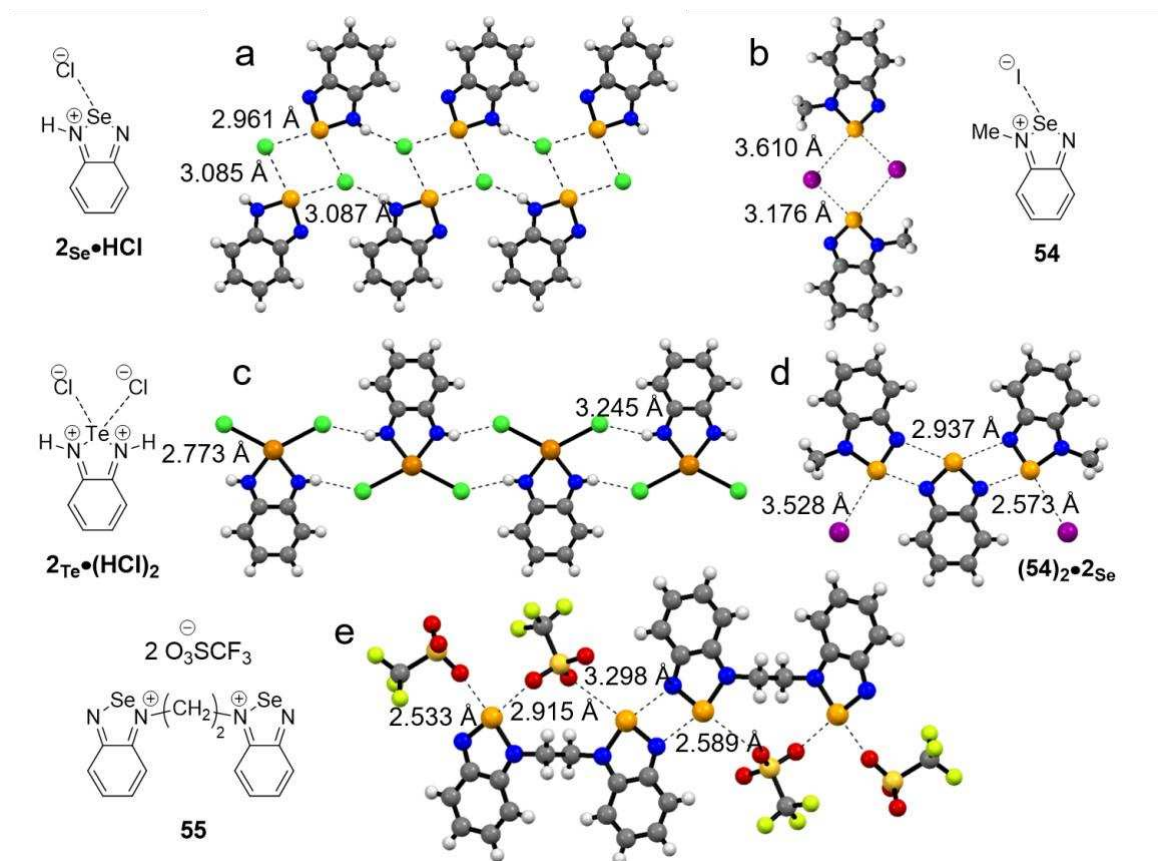
Figure 19: X-ray structures of chalcogenadiazolium salts: a) **2Se•HCl**,[89] b) **54**,[90] c) **2Te•(HCl)2** ,[89] d) **(54)2• 2Se** ,[90] and e) **55**.[91] Space groups: P$\bar{1}$ (**2Se•HCl**), b) P2₁/n (**54**), c) Pcca (**2Te•(HCl)2**), d) C2/c ((**54)2• 2Se**) and e) P$\bar{1}$ (**55**).

Interestingly, the X-ray structure of **2Se•HCl** shows the formation of supramolecular ribbons, each formed through a combination of multiple chalcogen- and hydrogen-bonds established between the Se- and N*H*-atoms ($d_{Cl…Se} = 2.961 – 3.085$ Å, $d_{Cl…N} = 3.087$ Å). While the benzo-1,2,5-selenadiazole leads to the formation of different crystalline materials depending on the stoichiometry of HCl, in the case of benzo-1,2,5-telluradiazole **2Te** only crystals of doubly-protonated **2Te•(HCl)2** could be obtained (Figure 19c). The X-ray structure shows the formation of ribbons that, similarly to the case of **2Se•HCl**, are formed through a combination of

chalcogen- and hydrogen-bonding interactions ($d_{Cl\dots Te}$ = 2.773 Å and $d_{Cl\dots N}$ = 3.245 Å). Another strategy used to strengthen the EBIs between benzo-1,2,5-selenadiazoles, consists in the alkylation of one of the N-atoms of the selenadiazole ring. Earlier examples have been reported by *Berionni et al.*[92] and *Risto et al.*[93], who methylated benzo-1,2,5-selenadiazoles with [Me$_3$O]BF$_4$. In their study, different salts have been prepared and crystallised, giving either crystals of pure **54** or co-crystals **(54)$_2$•2$_{Se}$** (Figures 19b and 19d). When molecule **54** is prepared and crystallised, the compound arranges in dimers through the formation of four bifurcated EBIs ($d_{I\dots Se}$ = 3.176 – 3.610 Å), in which I- anions act as bridging cornerstones between two molecules of **54** (Figure 19b). However, when **54** is reacted with less than an equivalent of [Me$_3$O]BF$_4$, supramolecular trimer **(54)$_2$•2$_{Se}$** is obtained, as confirmed by single-crystal X-ray measurements (Figure 19d). Trimer **(54)$_2$•2$_{Se}$** features N...Se short contacts ($d_{N\dots Se}$ = 2.573 - 2.937 Å) and terminal I...Se EBIs ($d_{I\dots Se}$ = 3.528 Å). In this oligomer, one molecule of **2$_{Se}$** is sandwiched between two molecules of **54**. Following a synthetic route in which the N-alkyl benzo-2,1,3-selenadiazolium cations are prepared by cyclo-condensation of the alkyl-phenylenediamine with selenous acid, *Vargas-Baca* and co-workers efficiently prepared a series of N-alkylated selenadiazolium cations and studied their self-assembly behaviours at the solid state.[90] Building on these results, the same group recently reported on the preparation of a bridged dicationic derivative, molecule **55**, and studied its potentialities to form polymers.[91] Surprisingly, the X-ray structure of crystals of **55** (Figure 19e) only showed the formation of doubly chalcogen-bonded dimers at a length of interaction considerably shorter than that observed in the crystalline solids of **2$_{Se}$** ($d_{N\dots Se}$ = 2.589 Å vs $d_{N\dots Se}$ = 3.155 Å). No supramolecular polymers were observed at the solid state. In an earlier work, the group also described the preparation and solid state assembly of acid-base Lewis adducts of **2$_{Te}$** with triphenylborane (BPh$_3$).[94, 95] Upon addition of either one or two equivalents of BPh$_3$ to a solution of **2$_{Te}$**, adducts bearing one (**2$_{Te}$•BPh$_3$**) or two (**2$_{Te}$•(BPh$_3$)$_2$**) borane derivatives could

be prepared. X-ray analysis of the crystals obtained for the 1:1 complex, showed that **2Te•BPh₃** self-assembles into dimers through squared double EBIs ($d_N{\ldots}_{Te}$ = 2.578 Å, Figure 20b). In these crystals, each molecule **2Te** engages in a N...B interaction between an N-atom and BPh₃, and the second occupied in an EBI with an adjacent Te centre. As expected, no EBIs were observed for **2Te•(BPh₃)₂**. When comparing the lengths of the chalcogen-bonds in the ribbon of **2Te** ($d_N{\ldots}_{Te}$ = 2.682-2.720 Å) with those measured for non-covalent dimer (**2Te•(BPh₃)**) ₂, one can notice that the EBIs formed by **2Te•(BPh₃)₂** are, stronger, *ca.* 0.1 Å shorter.
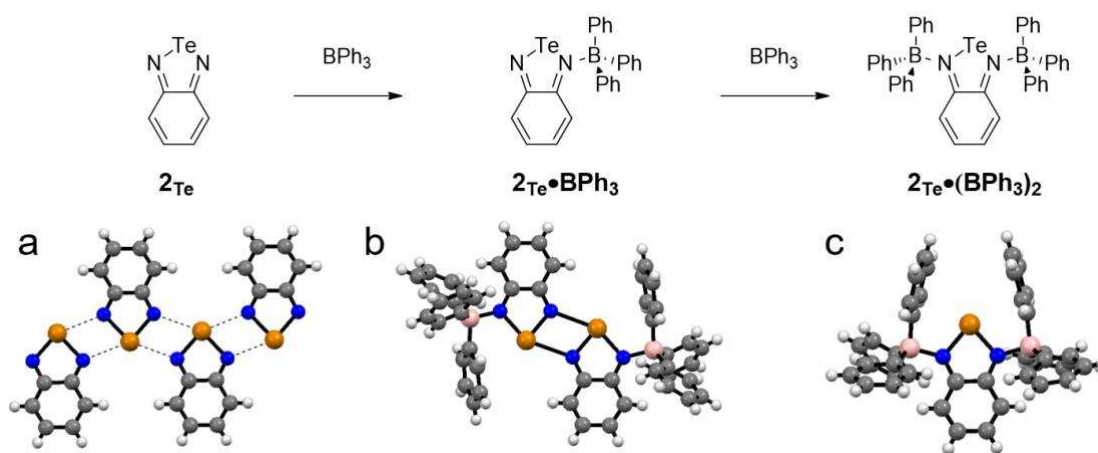
Figure 20: X-ray structure of a) **2Te** and of the adducts formed upon addition of b) one (**2Te•BPh₃**) and c) two (**2Te•(BPh₃)₂**) equivalents of BPh₃. Space groups: C2/c (**2Te**), P2₁/c (**2Te•BPh₃**) and P2₁/n (**2Te•(BPh₃)₂**).[81, 94]

3.2. 1,2-Chalcogenazole *N*-oxides: macrocyclic assembly

Beside the ribbon-like organisations at the solid state, the formation of tailored supramolecular structures through EBIs remains a challenge both in solution and at the solid state. In a seminal contribute, *Vargas-Baca* and co-workers conjectured that a 1,2-chalcogenazole *N*-oxide recognition motif could self-assemble in macrocycles through the formation of strong N-O...Te bonds.[96] The authors showed that 3-methyl-5-phenyl-1,2-tellurazole N-oxide **56** effectively undergoes self-assembly in solution to form macrocycles. The authors showed that, depending on the solvent of crystallisation, different supramolecular macrocycles could be obtained. For instance, compound **56** forms chains through EBIs ($d_O{\ldots}_{Te}$ = 2.176 – 2.207 Å) at the solid-state after slow evaporation of a benzene solution (Figure 21a).
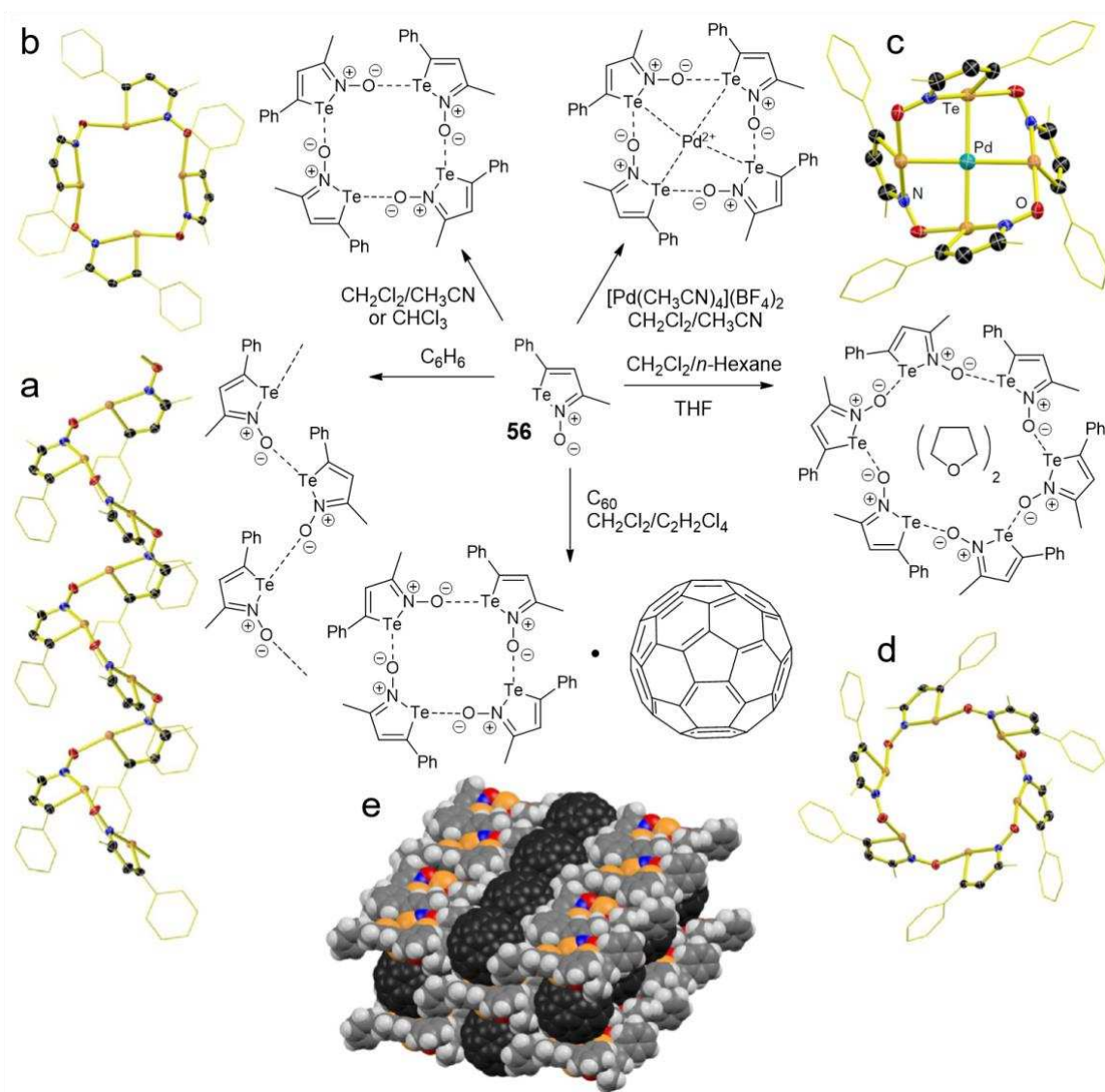
Figure 21: X-ray structure of **56** as a) linear chain (P2₁2₁2₁), b) cyclic tetramer (P$\bar{1}$), c) adduct with Pd(II) (I4₁/a), d) cyclic hexamer (R$\bar{3}$), e) inclusion complex with C₆₀ (C2/c).[96, 97] Adapted with permission from reference,[96] copyright 2016 Springer Nature.

When a MeCN/CH₂Cl₂ solution is mixed with [Pd(NCMe)₄](BF₄)₂, the complex [Pd(**56**)₄](BF₄)₂ is formed as characterised by X-ray diffraction analysis (Figure 21c). Cyclic tetramers (similarly to those of 3-methyl-5-(1,1-dimethylethyl)-Bu-1,2-tellurazole N-oxide)[97] could be formed ($d_{O\cdots Te}$ = 2.203 – 2.241 Å; Figure 21b) from evaporation of a CHCl₃ solution or slow diffusion of MeCN in a CH₂Cl₂ solution. Crystallisation of **56** from a THF solution leads to the formation of an inclusion compound in which a cyclic hexamer hosts a THF molecule (Figure 21d). At last, an hexameric structure is obtained from a CH₂Cl₂

solution. In this crystal, the solvent sits outside the cavities that are partially filled by two Me groups from neighbouring molecules. Interestingly, the structure of the tetrameric assembly and [Pd(**56**)4](BF4)2 could also be proven in solution by NMR and UV-vis absorption spectroscopic measurements. However, crystals of adduct **(56)4•C60** could only be achieved by slow diffusion of a solution of **C60** into a CHCl3 solution of **56** (Figure 21e). In this structure, the tellurazole N-oxide self-assembles in distorted boat-like six-membered rings, each hosting a C60 molecule. This unparalleled ability to form functional macrocycles through the self-association of simple building blocks shows the potential of the 1,2-tellurazole *N*-oxide as persistent supramolecular synthon. Those molecules have an ambidentate nature that is expressed in their capability of forming defined structures able to bind transition-metal ions. Following on this idea, the same group has very recently reported on the preparation and characterisation of coordination complexes.[98] The macrocycles successfully bind Cu(II) and Au(IV) cations in their tetrameric form, while Ag(I) cation has a preference for the hexamers.[98] Aiming at expanding the portfolio of molecular modules featuring the same auto-associative properties as that of **56,** *Vargas-Baca* and co-workers also reported the preparation of a benzo-1,2-chalcogenazole N-oxide (Figure 22). The crystal structures of **57E** show similar tetrameric, hexameric and linear patterns to those obtained for **56**. Molecules of **57Te** arrange in either tetrameric (Figure 22a) or hexameric (Figure 22b) macrocycles while crystallised from CH2Cl2/pyridine solution. On the other hand, Se-derivative **57Se** forms chains at the solid state (Figure 22c). Both molecules **56** and **57Te** simultaneously associate with Lewis acids (*e.g.* BF3) and bases (*e.g.*, DMAP, MeCN, biPy, PPh3 and carbene derivatives) at the solid state.[99]
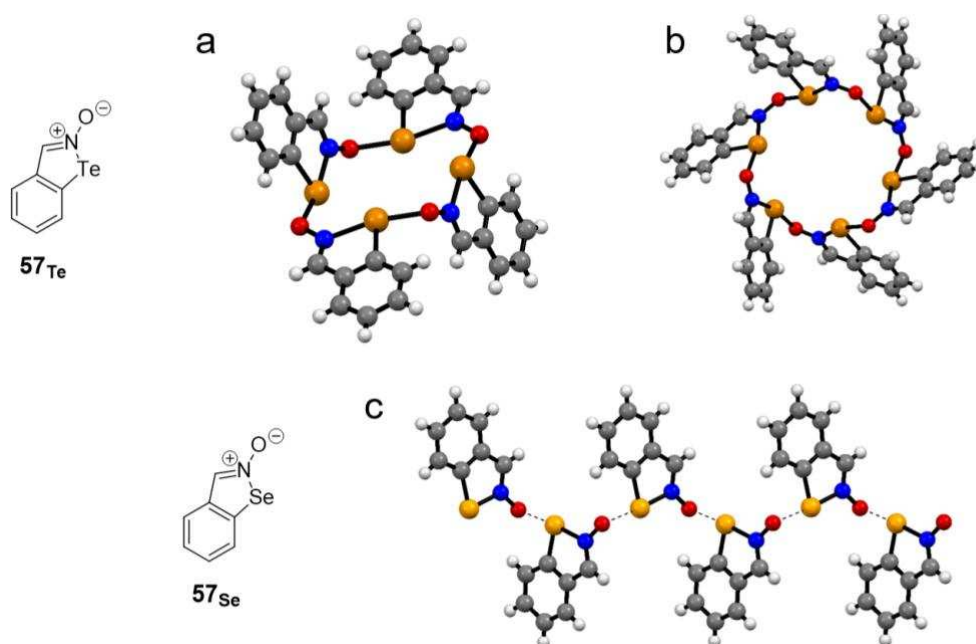
Figure 22: X-ray structure of **57E**: a) cyclic tetramer of **57Te**, b) cyclic hexamer of **57Te**, and c) linear chains of **57Se** (P2₁2₁2₁).[100] Space groups: P$\bar{1}$ (**57Te**), P3₁ (**57Te**), and P2₁2₁2₁ (**57Se**).

3.3. Wire-like structures formed by benzo-1,3-chalcogenazole

Our group contributed to the topic by engineering wire-like structures through single EBIs.[101] The key element of the work was the improvement of the synthesis of the benzo-1,3-selenazole motif over the reported literature procedures, and its generalisation to the Te-containing heterocycle.[102-106] The new synthetic pathway allow the derivatisation of the benzo-1,3-chalcogenazole scaffold at the 2-position with different functional groups.[101, 102] Indulging computational predictions of the electrostatic surface potentials (ESP) of different substrates using Gaussian 09 including the D01 revision, with the B97-D3/Def2-TZVP level of theory, we could program the self-assembly behavior at the solid-state of benzo-1,3-chalcogenazoles by tailoring the recognition properties of the chalcogen atom.[101] In these molecules, the EBI takes place between the most nucleophilic atom (*i.e.*, an N-atom) and one of the two σ-holes (*i.e.*, α and β) of an adjacent chalcogen atom. To favour the selectivity of the recognition, the σ-hole(β) can be blocked either by steric hindrance (steric tether) or electrostatically through an intramolecular EBI with a σ-hole stopper. This leaves the σ-hole(α)

free to engage with an electron donor atom. Phenyl substituents are sufficiently bulky to act as steric tethers, whereas 2-furanyl and 2-pyridyl as σ-hole electrostatic stoppers. Benzo-1,3-chalcogenazoles **58$_E$** have been synthesised bearing different substituents (*e.g.*, *i*-butyl, phenyl, furyl, thiophenyl, 2-pyridyl, 3-pyridyl, 4-pyridyl, styryl and ferrocenyl) in 2-position (Figure 23). Substituents bearing heteroatoms with negative $V_{s,max}$ values, such as 3- and 4-pyridyl moieties, act as tailored chalcogen-bond acceptors, overcoming the nucleophilic properties the azole N-atom, forming EBIs solely with the chalcogen through the σ-hole(α).[101]
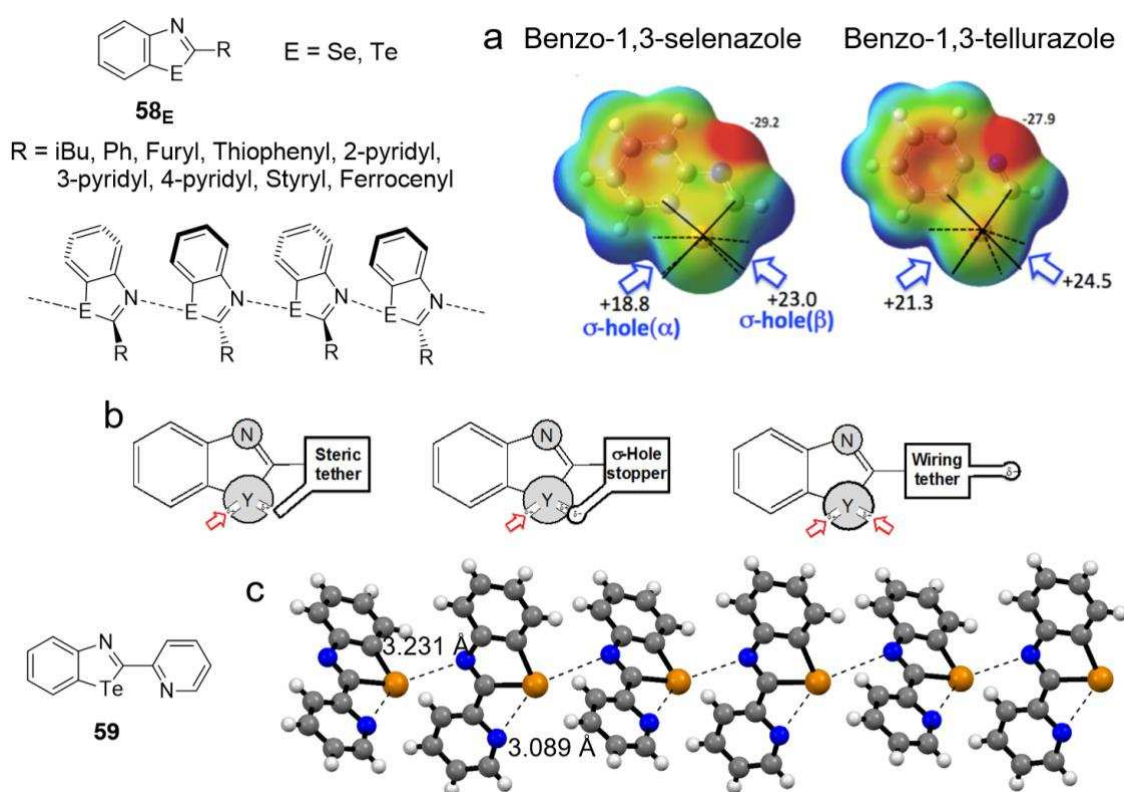
Figure 23: 2-Substituted benzo-1,3-chalcogenazole **58$_E$** forming wire-like structures through single EBIs, a) ESP map of benzo-1,3-selenazole and benzo-1,3-tellurazole, b) tailoring the molecular recognition properties of 2-substituted benzo-1,3-chalcogenazoles by obstruction of one σ-hole, c) X-ray structure of **59**, space group: Pca2₁. Adapted with permission from reference.[101]

Building on these results, we conjectured that the substitution of the benzo ring with a pyridyl ring as in the chalcogenazolopyrine scaffold (CGP), could allow the formation of dimeric structures at the solid state through self-complementary double EBIs (Figures 24a–c) arranged in a six-membered ring.[107] Se- and Te-bearing derivatives (i.e., with phenyl, pyridyl,

thiophenyl, trifluoro- and pentafluoro-phenyl substituents at the 2-position) were synthesised and their self-association at the solid-state probed by single-crystal X-ray diffraction analysis. The strongest recognition persistence was observed with the Te-congeners and strengthening of the interaction could be achieved with EWGs in 2-position (Figures 24d–f).[107] The Se-containing analogues featured a certain variability in their association at the solid-state, associating in dimers or supramolecular polymers through hydrogen-bonding interactions. Dimerisation through double EBIs was achieved only with strong EWGs such as pentafluorobenzene and CF_3 moieties.[107]
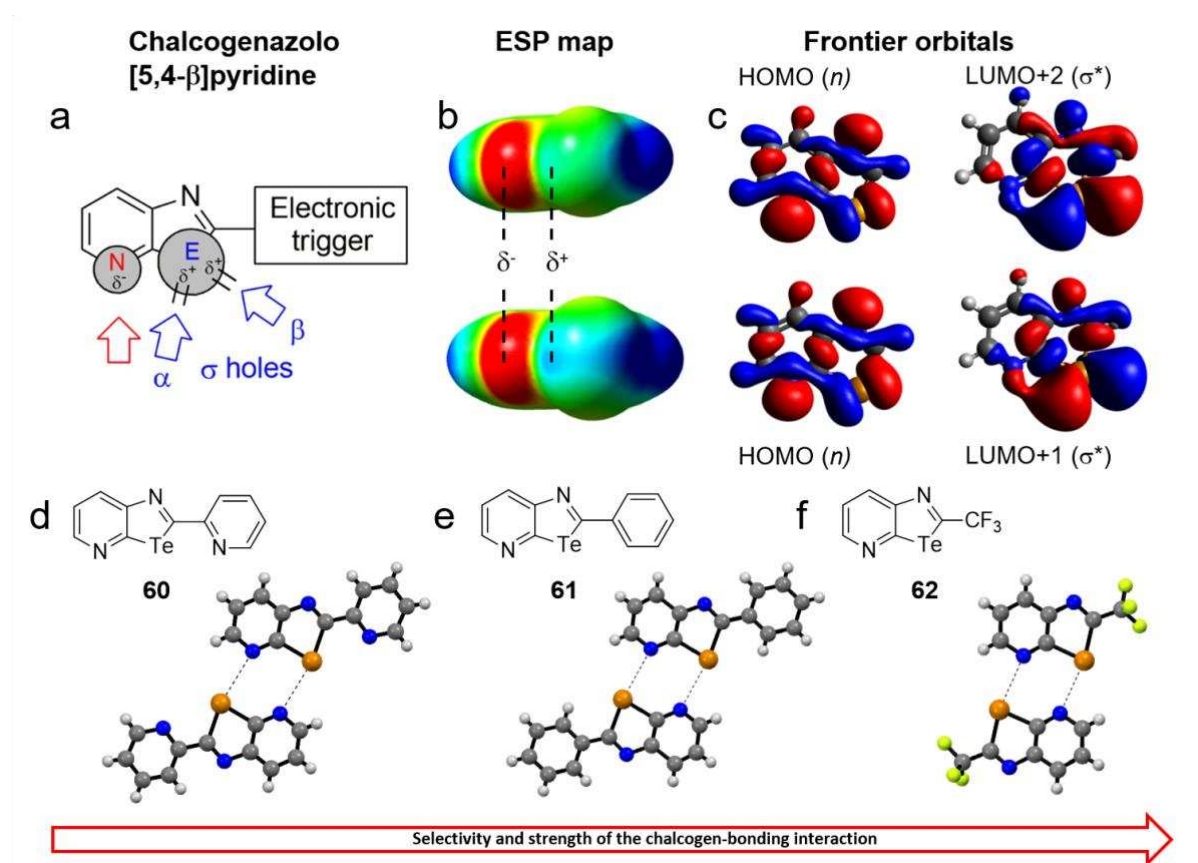
Figure 24: a) Basic scaffold of the chalcogenazolopyridine (CGP) motif; b) ESP map of [1,3]chalcogenazolo[5,4-b]pyridine (Se and Te at the top and bottom), c) relevant molecular orbitals, d-f) X-ray structure of (**60**)$_2$, (**61**)$_2$ and (**62**)$_2$. Reproduced with permission;[107] copyright 2018 Wiley-VCH Verlag GmbH & Co. KGaA, Weinheim.

Very recently, *Lu* et al.[108] computationally compared the CGP array to the dimers of 2,1,3-benzochalcogenadiazole, 1,2,5-chalcogenazolo-[3,4-*γ*]pyridine and 1,2,4-triazolo[3,4-*β*]-1,3,4-telluradiazole. Through the identification of the predominance of the electrostatic component

of the EBI in both systems, they proposed a two-parameter model that can predict the strength of the association using a potential of highest charge observed on the ESP map at the chalcogen (*i.e.*, σ-hole) and *N*-atoms.

3.4. Chalcogen-bonds meeting halogen-bonds: simultaneous expression of different SBIs

Selenadiazole derivatives have also shown potential applications in crystal engineering. Capitalising on the basicity exhibited by the two *N*-atoms of molecule **2Se**, co-crystals expressing hydrogen- and halogen-bonding interactions along with EBIs could be synthesised by *Gdaniec*, *Polonski* and co-workers (Figure 25).[109]
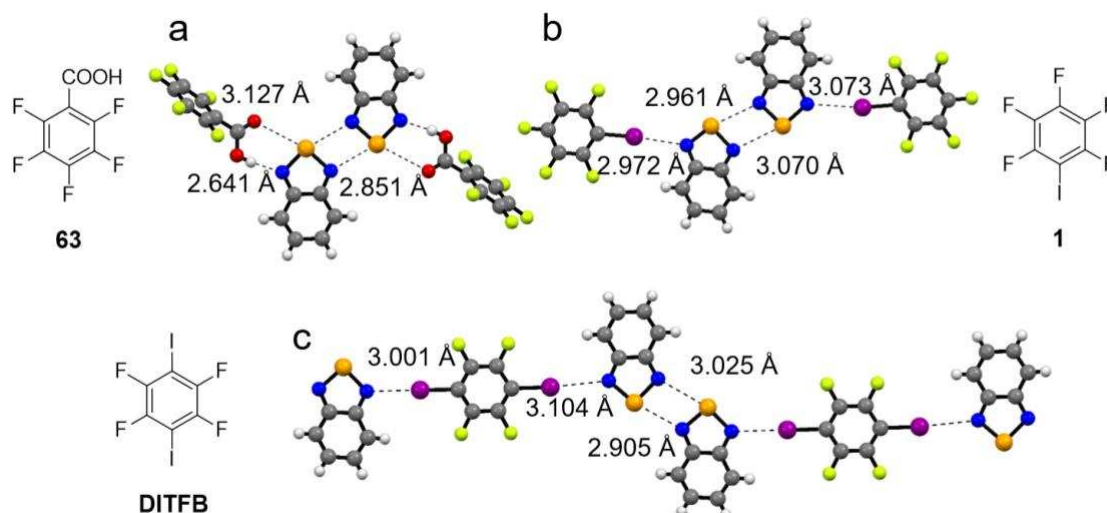
Figure 25: X-ray structure of co-crystals: a) **2Se•63**; b) **2Se•1**; c) **2Se•DITFB**. Space group: P2₁/c (**2Se•63**), P2₁/n (**2Se•1**) and P2₁/c (**2Se•DITFB**).[109]

The main feature of the assemblies lies in the formation of a dimeric **(2Se)₂** structures engaging with either a HB or XB donor. For example, co-crystals with perfluorobenzoic acid **63** show a tetrameric assembly **(2Se)₂•(63)₂** with four EBIs ($d_{O…Se}$ = 3.127 Å, $d_{N…Se}$ = 2.851 Å) and two HBIs ($d_{N…O}$ = 2.641 Å; Figure 25a). In a similar fashion, molecule **2Se** associates with perfluoroiodobenzene **1** to form supramolecular tetramers **(2Se)₂•(1)₂** (Figure 25b). Two units of **2Se** connect with each other through EBIs ($d_{N…Se}$ = 2.972 – 3.070 Å), while the free N-atoms engage with two molecules of **1** through a XBI ($d_{N…I}$ = 2.961 – 3.073 Å). At last, dimers of

2Se organise with the ditopic **DITFB** in a supramolecular polymer **((2Se)2•DITFB)n** through simultaneous XBIs and EBIs ($d_{N…I}$ = 3.025 – 3.104 Å and $d_{N…Se}$ = 2.905 – 3.001 Å, Figure 25c). As stated by the authors, the N-binding sites of **2Se** are identical, which may result in disruption of the dimers arrangement leading to a lack of control in the supramolecular architectures of higher complexity. Moving away from the 1,2,5-chalcogenadiazole motif, *Torubaev et al.* have successfully grown co-crystals of **DITFB** and diphenyl dichalcogenide **64E** (Figure 26).[110] At the solid state, pure **64Te** arranges in columnar structures through π–σ* interactions ($d_{C…Te}$ = 3.604 – 3.646 Å; Figure 26a), whereas congener **64Se** forms ribbons through Se...Se short contacts ($d_{Se…Se}$ = 3.726 Å; Figure 26b).
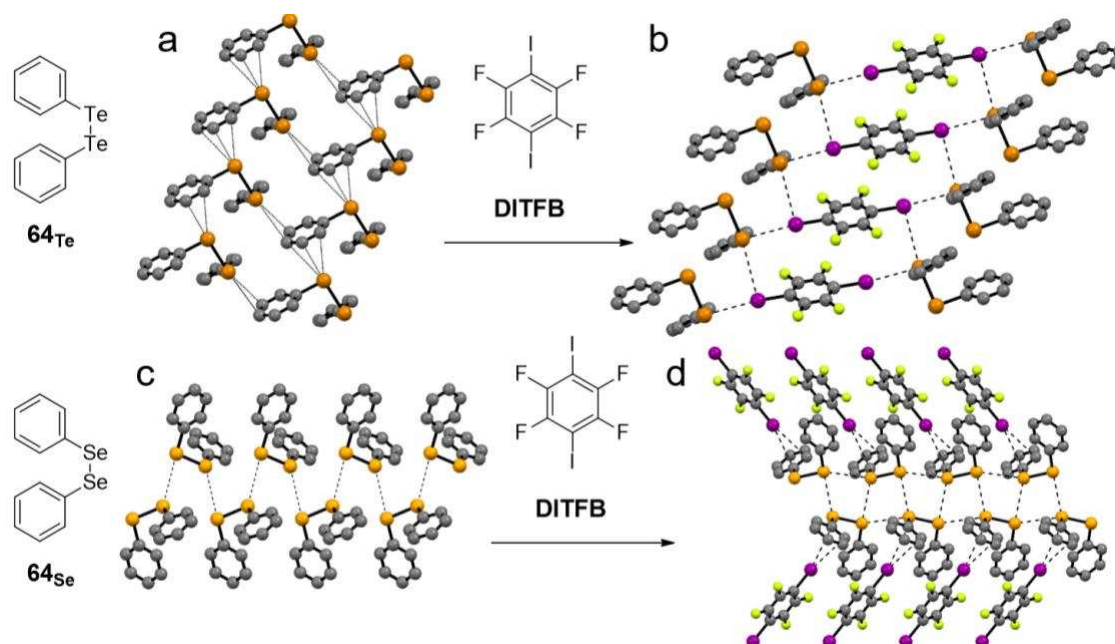
Figure 26: X-ray structure of **64E** and their respective co-crystal with **DITFB**. Space group: P2₁2₁2₁ for **64Te**, P2₁2₁2₁ for **64Se**, P2₁/n for **64Te•DITFB** and P2₁/c for **64Se•DITFB**.[110] H atoms are omitted for clarity.

Co-crystallisation of **64E** with **DITFB** leads to the insertion of the ditopic halogen-bond donor in the network of the dichalcogenide. In the case of the Te-congener, the columnar arrangement observed in the crystals of **64Te** is translated in the co-crystal with **DITFB** ($d_{C…Te}$ = 3.453 Å). However, in these crystals the columnar architectures connect with one another though **DITFB** molecules, which establish XBIs and EBIs involving both I- and Te-atoms ($d_{Te…I}$ = 3.574 Å and $d_{I…Te}$ = 4.031 Å, Figure 26c), respectively. For co-crystals of Se-analogue **64Se**, the ribbon

structure is tightened up ($d_{Se\cdots Se}$ = 3.752 Å and 3.606 Å), with **DITFB** units bridging each diselenide molecule through $\pi-\sigma^*$ interaction ($d_{C\cdots I}$ = 3.566 Å; Figure 26d).
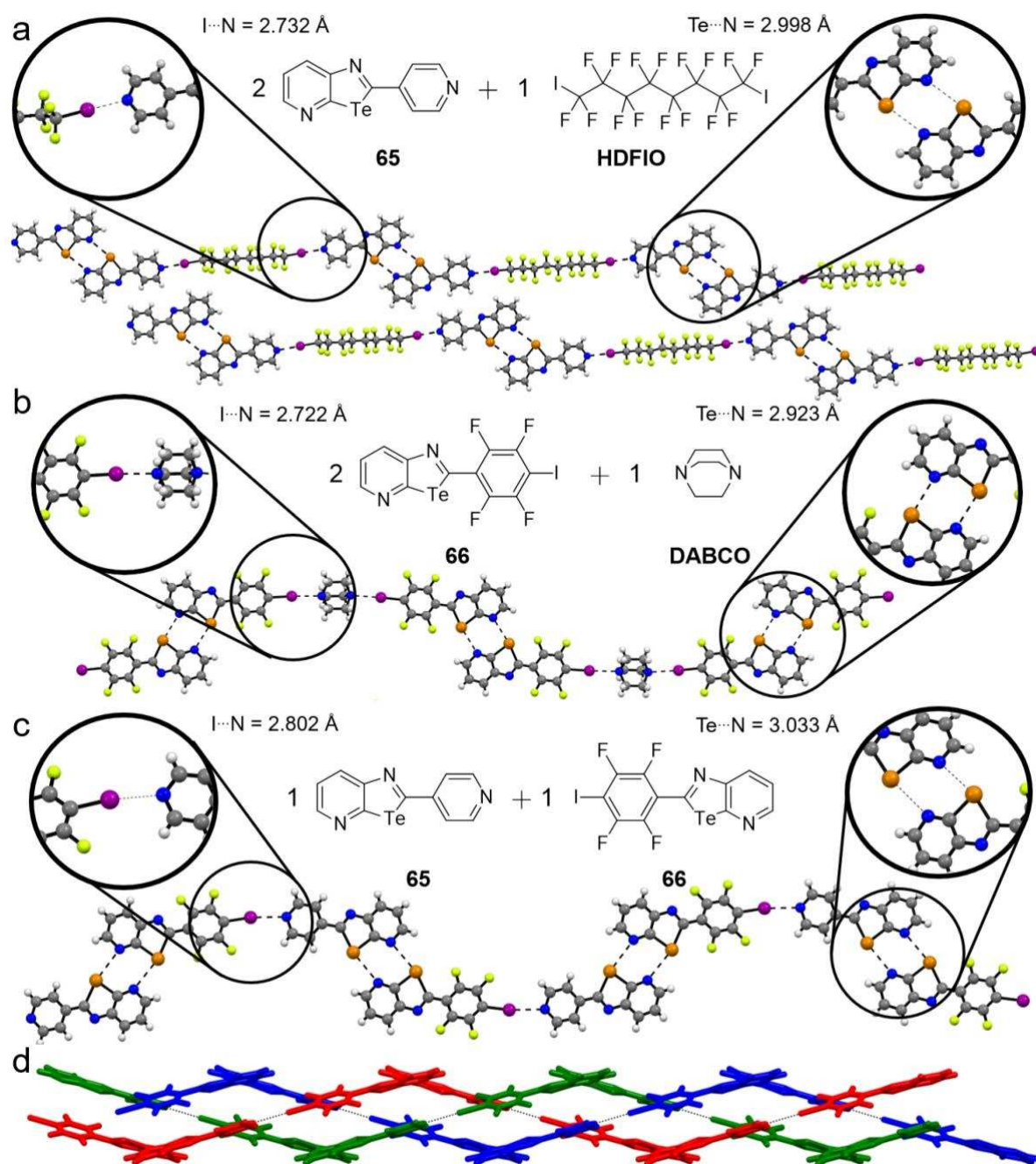
Figure 27: X-ray structures of co-crystals: a) **(65)₂•HDFIO**, b) **(66)₂•DABCO**, and c) **65•66**. d) Stick representation of the triple helix: each strain is highlighted in Red, Blue and Green. Space groups: P$\bar{1}$, P$\bar{1}$ and P2₁/n, respectively.

Very recently, our group also prepared crystalline multi-component solids through the simultaneous expression of both XBIs and EBIs.[111] Structurally-tailored supramolecular polymers at the solid state have been engineered through the programming of the CGP

recognition motif with either a halogen-bond acceptor (**65**) or donor (**66**) at the 2-position, which can interact with suitable complementary building blocks (*e.g.*, **HDFIO** and **DABCO**, Figure 27). The X-ray structure of co-crystal **65•HDFIO** shows that molecular units of **65** associate in pairs through double EBIs ($d_{N…Te} = 2.998$ Å),[107] with each dimer engaging with **HDFIO** *via* two XB contacts involving the pyrid-4-yl moieties ($d_{N…I} = 2.732$ Å, Figure 27a). Similar results could be obtained by inversing the halogen bond demand, as shown by the X-ray structure of co-crystal **66•DABCO** (Figure 27b). Molecule **66** dimerises through double EBIs ($d_{N…Te} = 2.923$ Å), with the dimers sandwiched between two **DABCO** through XBIs ($d_{N…I} = 2.722$ Å). At last, co-crystals **65•66** could be prepared by mixing the two derivatives in 1:1 stoichiometry (Figure 27c). Exceptionally, heteromolecular chalcogen-bonded dimers of **65** and **66** were formed ($d_{N…Te} = 3.033$ Å). Each dimer connects in a head-to-tail fashion through double EBIs ($d_{N…Te} = 2.702$ Å), giving a linear polymer that folds in a triple-helix superstructure (Figure 27d).

3.5. EBIs templating the formation of porous architecture

Certainly, one of the most appealing porous supramolecular architectures reported so far is that of *Gleiter* and co-workers, who described the formation of supramolecular nanotubes at the solid state using telluroethers.[19] Among the different architectures, one includes the supramolecular arrangement formed by 1,4- bis(methyltellanyl)buta-1,3-diyne **67** that, through EBIs, organise into helical channels featuring a square section (Figures 28b and 28c). In this case, each Te-atom behaves as both chalcogen-bond donor and acceptor, simultaneously engaging in four EBIs ($d_{Te…Te} = 3.741 – 3.824$ Å). When looking at the chalcogen atoms as chalcogen-bond acceptors, the angle between the two EBIs is around 110° (Figure 28a). Similar behaviour has been observed with cyclophanes[112] and cyclic tetra- and hexayne derivatives.[113] Chalcogen-chalcogen interactions have been also used to master the face-to-

face $\pi-\pi$ stacking of anthracene rings.[114] For a comprehensive review of these systems, we direct the interested reader to the recent account paper from the *Gleiter*'s group.[52]
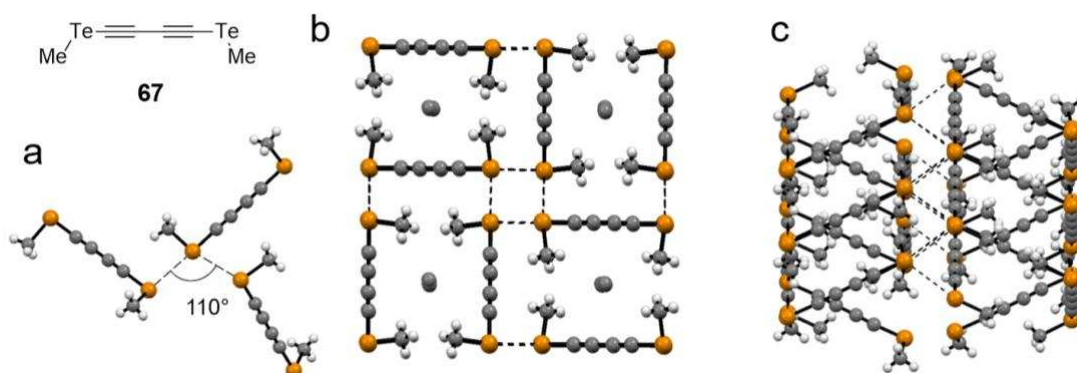
Figure 28: X-ray structure of diyne **67** and of its porous self-assembled structure.[19]

3.6. Conformational locking of organic semiconductors into planar backbones through EBIs.

Small-molecule and polymeric π-conjugated scaffolds are widely used for optoelectronic applications, especially in the field of flexible devices. Among all organic semiconductors, oligo-, poly-thiophenes and thienothiophenes stand out as versatile scaffolds in the field due to their easily-tuneable electronic bandgap, chemical stability, mechanical flexibility, light weight, and easy processability.[67, 115] In these linear π-conjugated systems, the HOMO-LUMO gap is controlled by five contributions: the deviation from planarity, the degree of bond length alternation, the resonance energy of the aromatic monomer units, the electronic effects of the substituents at the monomer units, and the intermolecular interactions between the chains in the solid state.[116] Although the bandgap of these systems mainly depends on degree of bond length alternation, the fact that single bonds are essentially linking the monomeric aromatic rings, inter-annular rotations can take place. Therefore, any significant deviations from coplanarity between the monomeric units will enhance the bandgap energies,[116-115] suggesting that any structural modifications that will lessen the rotational freedom between the monomeric aromatic rings will help the design of small bandgap linear π-conjugated frameworks.[115] In this contest, the use of any intramolecular EBIs involving the S-atoms of

the thiophene rings that, locking the linear π-conjugated framework into rigid planar conformation (Figure 29a), will allow the engineering of low-bandgap organic materials. One of the most striking examples is that of bi-(3,4-thylenedioxy)thiophene unit **68** (Figure 29b), in which two intramolecular O$_{...}$S EBIs (do…s = 2.920 Å) force the monomers to adopt a planar conformation. This increases the planarity and rigidity of the extended π-conjugated scaffold, enhancing the π-donor ability of the molecular scaffold.[115, 117, 118]
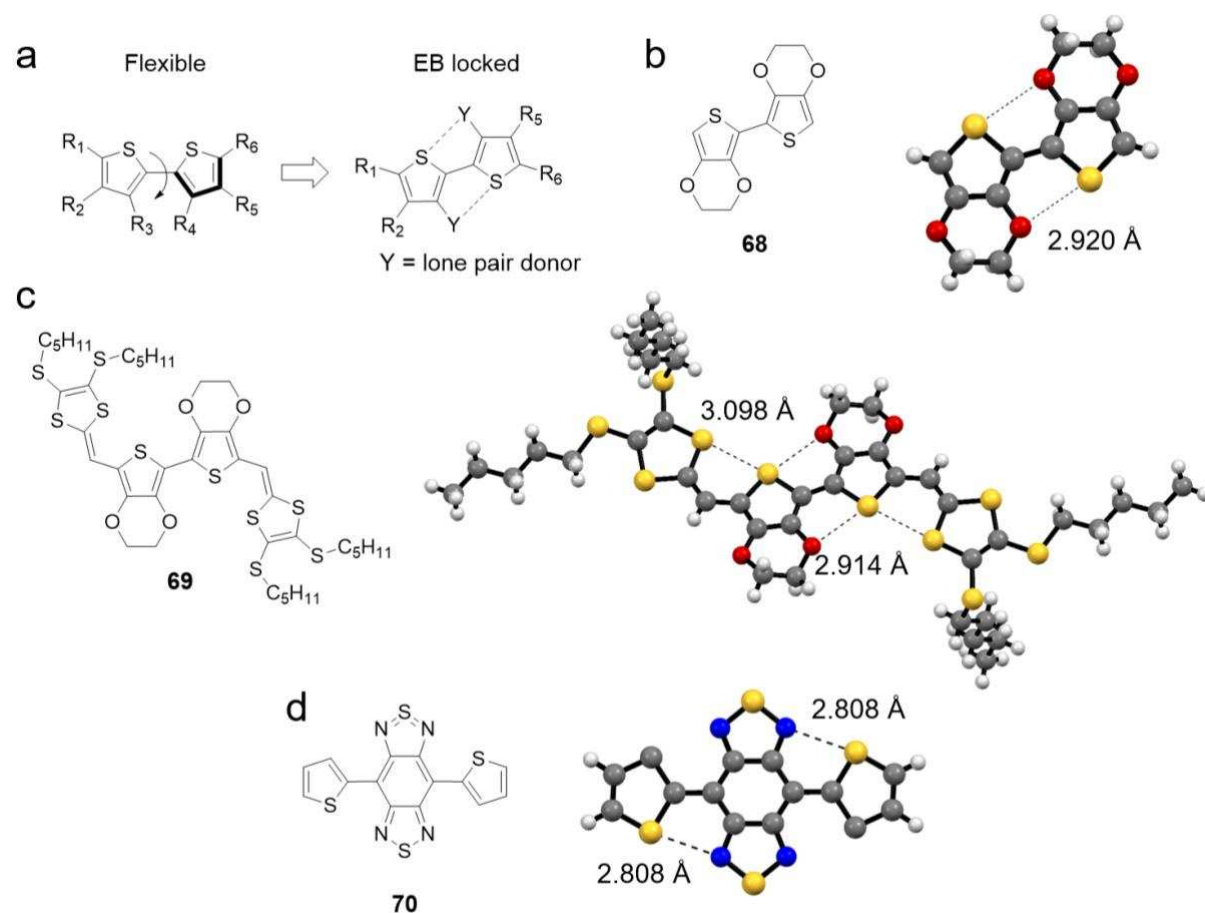
Figure 29: a) Conformational locking through intramolecular EBIs. X-ray structure of b) **68**,[118] c) **69**,[119] d) **70**.[126] Space groups: P2₁/c, P$\bar{1}$, P2₁/n, respectively.

The effect is also observed in the crystal structure of molecule **69**. For instance, the X-ray structure analysis of **69** revealed the presence of intramolecular O...S and S...S EBIs (do…s = 2.914 Å; ds…s = 3.098 Å, Figure 29c), which forced the π-conjugated rings to lye coplanar.[119] This locking effect has also been used in ifferent systems, including radical

cation salts,[120-122] tetrathiafulvalene-bithiophene hybrid conjugated systems,[123, 124] and small molecules constituted by thiadiazole and thiophene moieties.[125-127] Specifically, molecule **70** features a benzobis(1,2,5-thiadiazole) moiety containing hypervalent S-atoms and two thiophenyl units (Figure 29d), which are conformationally locked by intramolecular EBIs (d_N…s = 2.808 Å). For a comprehensive review on conformational locking interactions for polymeric semiconductors, we direct the interested reader to a recent review.[115]

3.7. EBIs-controlled self-assembly of organic morphologies at the microscale for optoelectronic applications.

Building on the EBI-driven conformational locking of oligothiophenes, the group of *Barbarella* and co-workers successfully engineered helicoidal fibres using an octathiophene derivative, the central tetrathiophene motif of which is functionalised with thioalkyl substituents at the 3-position of each thiophenyl unit (Figure 30).[128] Each lateral S-atom engage in an intramolecular EBI with the neighbouring thiophenyl S-atom (ds…s = 3.09 – 3.10 Å; Figure 30d), locking the central tetrathiophene core into a stable, flat prochiral conformation. The self-organisation of compounds **71**, **72** and **73** into fibres have been achieved by slow diffusion of MeCN to a solution of toluene dropped on a surface (*e.g.*, glass, ITO, silicon and gold). The crystalline assemblies have been characterised by scanning electron microscopy (Figures 30a-c), which depicted morphologies with a high aspect ratio (from 1:1 to 1:2 height *versus* width and length up to hundreds µm). When reference compound **74**, bearing hexyl chains at the place of S-hexyl substituents for **71**, was crystallised under the same conditions, only amorphous material was obtained. Taken all together these results suggest that the intramolecularly S...S locked central tetrathiophenyl prochiral core (Figure 30d) is the molecular algorithm that, when inserted in an oligothiophenyl, induces the fibrous arrangement. The reduction and oxidation potentials of the oligomers have been measured by cyclic voltammetry (E_{ox0} = 0.62 V and 0.60 V vs SCE, respectively and E_{red0} = -1.45 V and -1.52 V *vs* SCE, respectively). Organic field

effect transistors (OFETs) devices were built to measure the charge mobility along the fibrous morphologies. The fibres of molecules **71** and **72** have been characterised by hole mobility values of 9.8×10^{-7} and 5×10^{-6} cm^2 V^{-1} s^{-1}, respectively. Considering an effective coverage of 50%, a hole mobility value of 1×10^{-5} and 4×10^{-4} cm^2 V^{-1} s^{-1} has been calculated, which is two order of magnitude higher than the value observed for single fibres. Interestingly, fibres of both molecules **71** and **72** features intense red fluorescence, as observed by confocal microscopy.
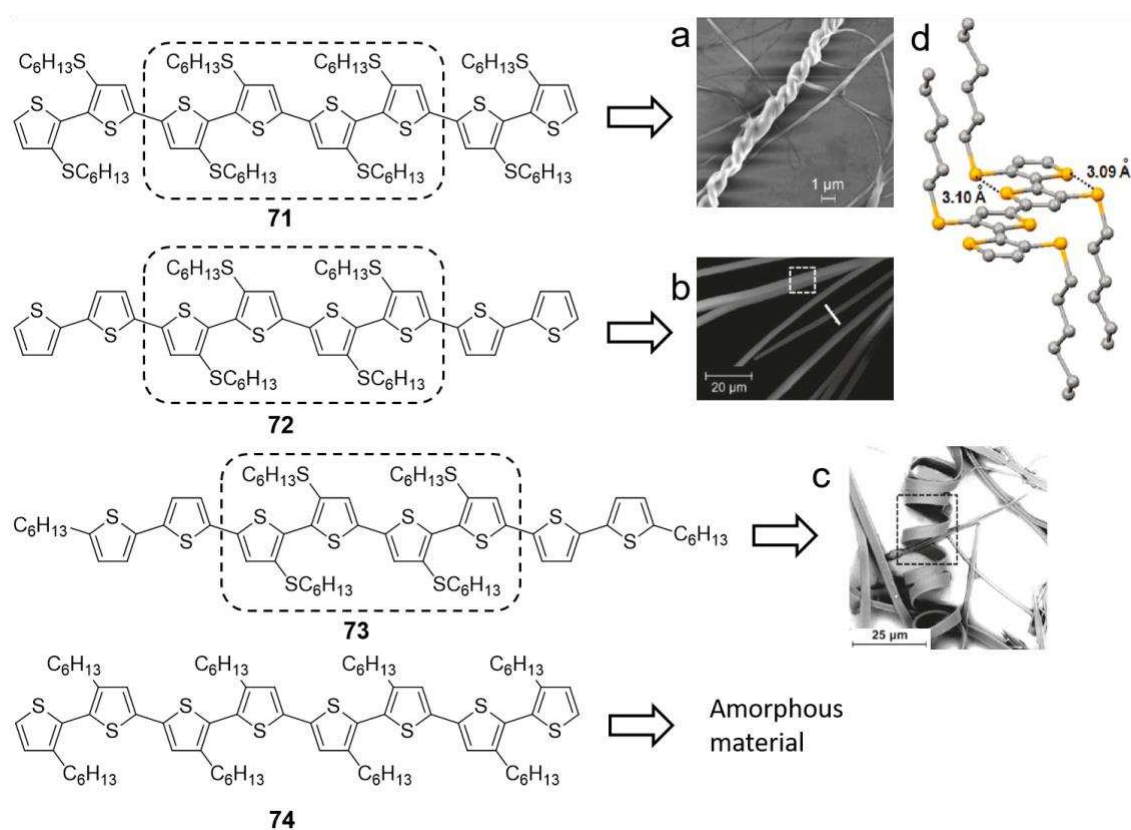
Figure 30: Oligothiophenes **71**-**74** substituted with alkyl and thioalkyl chains; the inner tetrameric core is contoured by dashed lines. SEM images of fibres of a) **72**, b) **73** and c) **74**. d) Preliminary X-ray structure of the tetrameric synthon. Adapted with permission from reference,[128] copyright 2011 American Chemical Society.

Thin films containing the fibres have been also investigated by small angle reflection of X-ray. The analysis suggested that the conformationally-locked planar octathiophenyl units arrange in *J*-type stacking organisation. The S$_{...}$S chalcogen bonds impose an anti-orientation of the thiophenes rings (as shown by preliminary single crystal X-ray diffraction analysis, Figure

30d). The same principle was then extended to different oligothiophenyl substrates, including oligothiophene,[129] bulk-heterojunction materials,[130] and conjugated polymers.[131]

4. Conclusions.

Going through the most topical and characteristic examples in the field, in this review, we report an overview of the theoretical and experimental studies unravelling the potentialities, prospects and challenges of exploiting chalcogen-bonding interactions in functional systems. The understanding and mastering of the association between molecular entities through EBIs are key points if one wants to design functional recognition arrays with chalcogen bonds. Therefore, in this paper we illustrated how progresses bloomed and are currently under development in the design and synthesis of programmed scaffolds undergoing chalcogen-bonding recognition to control new chemical systems for applications in supramolecular architectures, catalysis, and functional materials.

The use of EBIs in solution phases appeared in the 90's and evolved from anion recognition to catalysis. Unprecedented reactivity triggered by chalcogen-bonding has been discovered, such as in halogen-abstraction, hydrogenation reaction and activation of carbonyl groups in addition reactions. However, the use of EBIs to engineer non-covalent architectures from solution is scarce, with the most representative examples being the recently described supramolecular vesicles and capsules. In particular, the non-covalently assembled capsule represents the only example to date of a multiple chalcogen-bonded molecular architecture. At the solid-state, the most studied molecular modules are those bearing the 1,2,5-chalcogenadiazole moiety. Formation of tight associations as ribbons or discrete entities have been obtained with the Te-containing congeners, with the drawback of being moisture sensitive and thus not the ideal candidate for engineering functional materials for practical applications. While being more stable, the Se-doped analogues features weaker EBIs, which is also a limiting factor for their

integration into functional materials for practical application. Interestingly, crystalline materials simultaneously expressing EBIs and XBIs have been also reported, showing that the two SBIs are compatible and hold great potentialities for preparing responsible materials. Persistent recognition motifs such as 1,2-chalcogenazole N-oxide and the 1,3-chalcogenazole forming six-membered rings have been also recently developed, and emerged as chemically stable alternatives to the 1,2,5-chalcogenadiazole moiety for applications in crystal engineering. In materials science, chemists have used EBIs to control the rotational freedom between monomeric aromatic rings in linear π-conjugated systems. Locking linear oligo-, poly-thiophenes and thienothiophenes into rigid planar conformations through intramolecular EBIs involving the S-atoms of the thiophene rings, allowed the engineering of organic materials with tuneable low-bandgap properties.

From these combined experimental and theoretical efforts, it emerges that so far only arrays featuring single- and double-chalcogen bonding interactions have been developed, and their association is essentially governed by a combination of electrostatic, charge transfer ($n{\rightarrow}\sigma^*$ orbital-type interactions) and dispersion forces. In spite of these studies, the field is still far from a tailored design of programmed recognition motifs that, establishing multiple EBIs, can be exploited in supramolecular chemistry as previously done with multiple H-bonded arrays. The geometrical and physical requirements permitting the formation of multiple EBIs make the design of multiple EBIs arrays difficult, and further fundamental studies are still needed to establish those principles to program persistent self-assembling molecular synthons to be used in optoelectronic materials, sensing, catalysis, and drug discovery.

Together with the potentialities of forming supramolecular complexes with high association strengths, the complementary properties to classical non-covalent interactions, and the substantial orbital contribution to the interaction, EBI-based receptors can open to new opportunities for designing functional architectures for both biological applications and

materials science. This will help to advance closer to the objective of improving current materials performances or find alternative solutions for designing new multifunctional devices.

Bibliography.

[1] T. Chivers, R.S. Laitinen, Chem. Soc. Rev., 44 (2015) 1725-1739.

[2] C. E. Housecroft, A.G. Sharpe, in: Inorganic Chemistry, 4th ed., Pearson Education Ltd., Harlow, England, 2012.

[3] A.F. Cozzolino, P.J.W. Elder, I. Vargas-Baca, Coord. Chem. Rev., 255 (2011) 1426-1438.

[4] W.-W. duMont, C.G. Hrib, Handbook of Chalcogen Chemistry: New Perspectives in Sulfur, Selenium and Tellurium, 2nd ed., RSC Publishing, 2013.

[5] T.M. Beale, M.G. Chudzinski, M.G. Sarwar, M.S. Taylor, Chem. Soc. Rev., 42 (2013) 1667-1680.

[6] R. Bertani, P. Sgarbossa, A. Venzo, F. Lelj, M. Amati, G. Resnati, T. Pilati, P. Metrangolo, G. Terraneo, Coord. Chem. Rev., 254 (2010) 677-695.

[7] L.C. Gilday, S.W. Robinson, T.A. Barendt, M.J. Langton, B.R. Mullaney, P.D. Beer, Chem. Rev., 115 (2015) 7118-7195.

[8] E. Persch, O. Dumele, F. Diederich, Angew. Chem. Int. Ed., 54 (2015) 3290-3327.

[9] P. Metrangolo, F. Meyer, T. Pilati, G. Resnati, G. Terraneo, Angew. Chem. Int. Ed., 47 (2008) 6114-6127.

[10] T. Clark, M. Hennemann, J.S. Murray, P. Politzer, J. Mol. Model., 13 (2007) 291-296.

[11] M. Erdelyi, Chem. Soc. Rev., 41 (2012) 3547-3557.

[12] M. Cametti, B. Crousse, P. Metrangolo, R. Milani, G. Resnati, Chem. Soc. Rev., 41 (2012) 31-42.

[13] P. Metrangolo, G. Resnati, Nat. Chem., 4 (2012) 437-438.

[14] M.J. Langton, S.W. Robinson, I. Marques, V. Felix, P.D. Beer, Nat. Chem., 6 (2014) 1039-1043.

[15] G. Cavallo, P. Metrangolo, T. Pilati, G. Resnati, M. Sansotera, G. Terraneo, Chem. Soc. Rev., 39 (2010) 3772-3783.

[16] E. Parisini, P. Metrangolo, T. Pilati, G. Resnati, G. Terraneo, Chem. Soc. Rev., 40 (2011) 2267-2278.

[17] R. Berger, G. Resnati, P. Metrangolo, E. Weber, J. Hulliger, Chem. Soc. Rev., 40 (2011) 3496-3508.

[18] Á.M. Montaña, ChemistrySelect, 2 (2017) 9094-9112.

[19] D.B. Werz, R. Gleiter, F. Rominger, J. Am. Chem. Soc., 124 (2002) 10638-10639.

[20] J.S. Murray, P. Lane, P. Politzer, Int. J. Quantum Chem., 107 (2007) 2286-2292.

[21] B. Aakeroy Christer, L. Bryce David, R. Desiraju Gautam, A. Frontera, C. Legon Anthony, F. Nicotra, K. Rissanen, S. Scheiner, G. Terraneo, P. Metrangolo, G. Resnati, in: Pure and Applied Chemistry, 2019, pp. 1889.

[22] P. Politzer, J.S. Murray, P. Lane, Int. J. Quantum Chem., 107 (2007) 3046-3052.

[23] S. Zhu, C. Xing, W. Xu, G. Jin, Z. Li, Cryst. Growth Des., 4 (2004) 53-56.

[24] A. Priimagi, G. Cavallo, A. Forni, M. Gorynsztejn–Leben, M. Kaivola, P. Metrangolo, R. Milani, A. Shishido, T. Pilati, G. Resnati, G. Terraneo, Adv. Funct. Mater., 22 (2012) 2572-2579.

[25] A. Mukherjee, S. Tothadi, G.R. Desiraju, Acc. Chem. Res., 47 (2014) 2514-2524.

[26] S. Scheiner, Struct. Chem., 30 (2019) 1119-1128.

[27] E. Corradi, S.V. Meille, M.T. Messina, P. Metrangolo, G. Resnati, Angew. Chem. Int. Ed., 39 (2000) 1782-1786.

[28] H.A. Bent, Chem. Rev., 68 (1968) 587-648.

[29] J.Y.C. Lim, P.D. Beer, Chem, 4 (2018) 731-783.

[30] I. Vargas-Baca, T. Chivers, Phosphorus Sulfur Silicon Relat. Elem., 164 (2000) 207-227.

[31] A.F. Cozzolino, I. Vargas-Baca, Cryst. Growth Des., 11 (2011) 668-677.

[32] A. Jolleys, W. Levason, G. Reid, Dalton Trans., 42 (2013) 2963-2972.

[33] A.F. Cozzolino, I. Vargas-Baca, S. Mansour, A.H. Mahmoudkhani, J. Am. Chem. Soc., 127 (2005) 3184-3190.

[34] C. Cohen-Addad, M.S. Lehmann, P. Becker, L. Parkanyi, A. Kalman, J. Chem. Soc., Perkin Trans. 2, (1984) 191-196.

[35] R.E. Rosenfield, Jr., R. Parthasarathy, J.D. Dunitz, J. Am. Chem. Soc., 99 (1977) 4860-4862.

[36] J. Fanfrlik, A. Prada, Z. Padelkova, A. Pecina, J. Machacek, M. Lepsik, J. Holub, A. Ruzicka, D. Hnyk, P. Hobza, Angew. Chem. Int. Ed., 53 (2014) 10139-10142.

[37] T.N.G. Row, R. Parthasarathy, J. Am. Chem. Soc., 103 (1981) 477-479.

[38] G.E. Garrett, G.L. Gibson, R.N. Straus, D.S. Seferos, M.S. Taylor, J. Am. Chem. Soc., 137 (2015) 4126-4133.

[39] F. De Vleeschouwer, M. Denayer, B. Pinter, P. Geerlings, F. De Proft, J. Comput. Chem., 39 (2018) 557-572.

[40] D.J. Pascoe, K.B. Ling, S.L. Cockroft, J. Am. Chem. Soc., 139 (2017) 15160-15167.

[41] P.L. Bora, M. Novák, J. Novotný, C. Foroutan-Nejad, R. Marek, Chem. Eur. J., 23 (2017) 7315-7323.

[42] S. Bhandary, A. Sirohiwal, R. Kadu, S. Kumar, D. Chopra, Cryst. Growth Des., 18 (2018) 3734-3739.

[43] M.R. Ams, N. Trapp, A. Schwab, J.V. Milić, F. Diederich, Chem. Eur. J., 25 (2019) 323-333.

[44] P. Politzer, J.S. Murray, M.C. Concha, J. Mol. Model., 14 (2008) 659-665.

[45] L. Brammer, Faraday Discuss., 203 (2017) 485-507.

[46] C. Bleiholder, R. Gleiter, D.B. Werz, H. Köppel, Inorg. Chem., 46 (2007) 2249-2260.

[47] C. Bleiholder, D.B. Werz, H. Köppel, R. Gleiter, J. Am. Chem. Soc., 128 (2006) 2666-2674.

[48] E. Alikhani, F. Fuster, B. Madebene, S.J. Grabowski, Phys. Chem. Chem. Phys., 16 (2014) 2430-2442.

[49] M.E. Brezgunova, J. Lieffrig, E. Aubert, S. Dahaoui, P. Fertey, S. Lebègue, J.G. Ángyán, M. Fourmigué, E. Espinosa, Cryst. Growth Des., 13 (2013) 3283-3289.

[50] S. Tsuzuki, N. Sato, J. Phys. Chem. B, 117 (2013) 6849-6855.

[51] W. Wang, B. Ji, Y. Zhang, J. Phys. Chem. A, 113 (2009) 8132-8135.

[52] R. Gleiter, G. Haberhauer, D.B. Werz, F. Rominger, C. Bleiholder, Chem. Rev., 118 (2018) 2010-2041.

[53] N.A. Semenov, A.V. Lonchakov, N.P. Gritsan, A.V. Zibarev, Russ. Chem. Bull. Int. Ed., 64 (2015) 499-510.

[54] K.T. Mahmudov, M.N. Kopylovich, M.F.C. Guedes da Silva, A.J.L. Pombeiro, Dalton Trans., 46 (2017) 10121-10138.

[55] L. Vogel, P. Wonner, S.M. Huber, Angew. Chem. Int. Ed., 58 (2019) 1880-1891.

[56] H. Zhao, F.P. Gabbaï, Nat. Chem., 2 (2010) 984-990.

[57] E.A. Suturina, N.A. Semenov, A.V. Lonchakov, I.Y. Bagryanskaya, Y.V. Gatilov, I.G. Irtegova, N.V. Vasilieva, E. Lork, R. Mews, N.P. Gritsan, A.V. Zibarev, J. Phys. Chem. A, 115 (2011) 4851-4860.

[58] N.A. Semenov, N.A. Pushkarevsky, J. Beckmann, P. Finke, E. Lork, R. Mews, I.Y. Bagryanskaya, Y.V. Gatilov, S.N. Konchenko, V.G. Vasiliev, A.V. Zibarev, Eur. J. Inorg. Chem., 2012 (2012) 3693-3703.

[59] N.A. Semenov, A.V. Lonchakov, N.A. Pushkarevsky, E.A. Suturina, V.V. Korolev, E. Lork, V.G. Vasiliev, S.N. Konchenko, J. Beckmann, N.P. Gritsan, A.V. Zibarev, Organomet., 33 (2014) 4302-4314.

[60] G.E. Garrett, E.I. Carrera, D.S. Seferos, M.S. Taylor, Chem. Commun., 52 (2016) 9881-9884.

[61] J.Y.C. Lim, I. Marques, A.L. Thompson, K.E. Christensen, V. Félix, P.D. Beer, J. Am. Chem. Soc., 139 (2017) 3122-3133.

[62] J.Y.C. Lim, J.Y. Liew, P.D. Beer, Chem. Eur. J., 24 (2018) 14560-14566.

[63] A. Borissov, I. Marques, J.Y.C. Lim, V. Félix, M.D. Smith, P.D. Beer, J. Am. Chem. Soc., 141 (2019) 4119-4129.

[64] J.Y.C. Lim, I. Marques, V. Félix, P.D. Beer, Chem. Commun., 54 (2018) 10851-10854.

[65] S. Benz, M. Macchione, Q. Verolet, J. Mareda, N. Sakai, S. Matile, J. Am. Chem. Soc., 138 (2016) 9093-9096.

[66] M. Macchione, M. Tsemperouli, A. Goujon, A.R. Mallia, N. Sakai, K. Sugihara, S. Matile, Helv. Chim. Acta, 101 (2018) e1800014.

[67] K. Strakova, L. Assies, A. Goujon, F. Piazzolla, H.V. Humeniuk, S. Matile, Chem. Rev., 119 (2019) 10977-11005.

[68] L.M. Lee, M. Tsemperouli, A.I. Poblador-Bahamonde, S. Benz, N. Sakai, K. Sugihara, S. Matile, J. Am. Chem. Soc., 141 (2019) 810-814.

[69] J. Bamberger, F. Ostler, O.G. Mancheño, ChemCatChem, 11 (2019) 5198-5211.

[70] (a) S. Benz, J. López-Andarias, J. Mareda, N. Sakai, S. Matile, Angew. Chem. Int. Ed., 56 (2017) 812-815; (b) S. Benz, J. Mareda, C. Besnard, N. Sakai, S. Matile, Chem. Sci., 8 (2017) 8164-8169

[71] (a) P. Wonner, L. Vogel, M. Düser, L. Gomes, F. Kniep, B. Mallick, D.B. Werz, S.M. Huber, Angew. Chem. Int. Ed., 56 (2017) 12009-12012; (b) P. Wonner, L. Vogel, F. Kniep,

S.M. Huber, Chem. Eur. J., 23 (2017) 16972-16975; (c) P. Wonner, A. Dreger, L. Vogel, E. Engelage, S.M. Huber, Angew. Chem. Int. Ed., 58 (2019) 16923-16927; (d) P. Wonner, T. Steinke, L. Vogel, S.M. Huber, Chem. Eur. J., 26 (2020) 1258-1262.

[72] C.M. Young, A. Elmi, D.J. Pascoe, R.K. Morris, C. McLaughlin, A.M. Woods, A.B. Frost, A. de la Houpliere, K.B. Ling, T.K. Smith, A.M.Z. Slawin, P.H. Willoughby, S.L. Cockroft, A.D. Smith, Angew. Chem. Int. Ed., 58 (2020) DOI: 10.1002/anie.201914421.

[73] (a) W. Wang, H. Zhu, L. Feng, Q. Yu, J. Hao, R. Zhu, Y. Wang, J. Am. Chem. Soc., 142 (2020) DOI: 10.1021/jacs.9b12610; (b) R. Weiss, E. Aubert, P. Peluso, S. Cossu, P. Pale, V. Mamane, Molecules 24, (2019) 4484.

[74] S. Benz, A.I. Poblador-Bahamonde, N. Low-Ders, S. Matile, Angew. Chem. Int. Ed., 57 (2018) 5408-5412.

[75] W. Wang, H. Zhu, S. Liu, Z. Zhao, L. Zhang, J. Hao, Y. Wang, J. Am. Chem. Soc., 141 (2019) 9175-9179.

[76] L. Chen, J. Xiang, Y. Zhao, Q. Yan, J. Am. Chem. Soc., 140 (2018) 7079-7082.

[77] L.-J. Riwar, N. Trapp, K. Root, R. Zenobi, F. Diederich, Angew. Chem. Int. Ed., 57 (2018) 17259-17264.

[78] O. Dumele, N. Trapp, F. Diederich, Angew. Chem. Int. Ed., 54 (2015) 12339-12344.

[79] O. Dumele, B. Schreib, U. Warzok, N. Trapp, C.A. Schalley, F. Diederich, Angew. Chem. Int. Ed., 56 (2017) 1152-1157.

[80] P. Scilabra, G. Terraneo, G. Resnati, Acc. Chem. Res., 52 (2019) 1313-1324.

[81] A.F. Cozzolino, J.F. Britten, I. Vargas-Baca, Cryst. Growth Des., 6 (2006) 181-186.

[82] R. Neidlein, D. Knecht, H. Endres, in: Zeitschrift für Naturforschung B, 1987, pp. 84.

[83] T. Chivers, X. Gao, M. Parvez, Inorg. Chem., 35 (1996) 9-15.

[84] A.F. Cozzolino, Q. Yang, I. Vargas-Baca, Cryst. Growth Des., 10 (2010) 4959-4964.

[85] A.F. Cozzolino, I. Vargas-Baca, J. Organomet. Chem., 692 (2007) 2654-2657.

[86] A.C. Gomes, G. Biswas, A. Banerjee, W.L. Duax, Acta Crystallogr. Sect. C, 45 (1989) 73-75.

[87] P.B. Pati, S.S. Zade, Cryst. Growth Des., 14 (2014) 1695-1700.

[88] S. Mondal, M. Konda, B. Kauffmann, M.K. Manna, A.K. Das, Cryst. Growth Des., 15 (2015) 5548-5554.

[89] L.M. Lee, P.J.W. Elder, A.F. Cozzolino, Q. Yang, I. Vargas-Baca, Main Group Chem., 9 (2010) 117-133.

[90] L.M. Lee, V.B. Corless, M. Tran, H. Jenkins, J.F. Britten, I. Vargas-Baca, Dalton Trans., 45 (2016) 3285-3293.

[91] L.M. Lee, V. Corless, H. Luu, A. He, H. Jenkins, J.F. Britten, F. Adam Pani, I. Vargas-Baca, Dalton Trans., 48 (2019) 12541-12548.

[92] G. Berionni, B. Pégot, J. Marrot, R. Goumont, Cryst. Eng. Comm., 11 (2009) 986-988.

[93] M. Risto, R.W. Reed, C.M. Robertson, R. Oilunkaniemi, R.S. Laitinen, R.T. Oakley, Chem. Commun., (2008) 3278-3280.

[94] A.F. Cozzolino, A.D. Bain, S. Hanhan, I. Vargas-Baca, Chem. Commun., (2009) 4043-4045.

[95] J. Lee, L.M. Lee, Z. Arnott, H. Jenkins, J.F. Britten, I. Vargas-Baca, New J. Chem., 42 (2018) 10555-10562.

[96] P.C. Ho, P. Szydlowski, J. Sinclair, P.J.W. Elder, J. Kubel, C. Gendy, L.M. Lee, H. Jenkins, J.F. Britten, D.R. Morim, I. Vargas-Baca, Nat. Commun., 7 (2016) 11299.

[97] J. Kübel, P.J.W. Elder, H.A. Jenkins, I. Vargas-Baca, Dalton Trans., 39 (2010) 11126-11128.

[98] J. Wang, P.C. Ho, J.F. Britten, V. Tomassetti, I. Vargas-Baca, New J. Chem., (2019).

[99] P.C. Ho, H.A. Jenkins, J.F. Britten, I. Vargas-Baca, Faraday Discuss., 203 (2017) 187-199.

[100] P.C. Ho, J. Rafique, J. Lee, L.M. Lee, H.A. Jenkins, J.F. Britten, A.L. Braga, I. Vargas-Baca, Dalton Trans., 46 (2017) 6570-6579.

[101] A. Kremer, A. Fermi, N. Biot, J. Wouters, D. Bonifazi, Chem. Eur. J., 22 (2016) 5665-5675.

[102] A. Kremer, C. Aurisicchio, F. De Leo, B. Ventura, J. Wouters, N. Armaroli, A. Barbieri, D. Bonifazi, Chem. Eur. J., 21 (2015) 15377-15387.

[103] M. Mbuyi, M. Evers, G. Tihange, A. Luxen, L. Christiaens, Tetrahedron Lett., 24 (1983) 5873-5876.

[104] C.S. Radatz, D. Alves, P.H. Schneider, Tetrahedron, 69 (2013) 1316-1321.

[105] S. Redon, Y. Kabri, M.D. Crozet, P. Vanelle, Tetrahedron Lett., 55 (2014) 5052-5054.

[106] T. Su, S. Xie, B. Li, J. Yan, L. Huang, X. Li, Synlett, 26 (2015) 215-220.

[107] N. Biot, D. Bonifazi, Chem. Eur. J., 24 (2018) 5439-5443.

[108] Y. Lu, W. Li, W. Yang, Z. Zhu, Z. Xu, H. Liu, Phys. Chem. Chem. Phys., 21 (2019) 21568-21576.

[109] K. Eichstaedt, A. Wasilewska, B. Wicher, M. Gdaniec, T. Połoński, Cryst. Growth Des., 16 (2016) 1282-1293.

[110] Y.V. Torubaev, D.K. Rai, I.V. Skabitsky, S. Pakhira, A. Dmitrienko, New J. Chem., 43 (2019) 7941-7949.

[111] N. Biot, D. Bonifazi, Chem. Eur. J., (2020) DOI: 10.1002/chem.201904762.

[112] D.B. Werz, F.R. Fischer, S.C. Kornmayer, F. Rominger, R. Gleiter, J. Org. Chem., 73 (2008) 8021-8029.

[113] D.B. Werz, R. Gleiter, F. Rominger, J. Org. Chem., 69 (2004) 2945-2952.

[114] K. Kobayashi, H. Masu, A. Shuto, K. Yamaguchi, Chem. Mater., 17 (2005) 6666-6673.

[115] H. Huang, L. Yang, A. Facchetti, T.J. Marks, Chem. Rev., 117 (2017) 10291-10318.

[116] J. Roncali, Chem. Rev., 97 (1997) 173-206.

[117] M. Turbiez, P. Frère, P. Blanchard, J. Roncali, Tetrahedron Lett., 41 (2000) 5521-5525.

[118] J.-M. Raimundo, P. Blanchard, P. Frère, N. Mercier, I. Ledoux-Rak, R. Hierle, J. Roncali, Tetrahedron Lett., 42 (2001) 1507-1510.

[119] P. Leriche, M. Turbiez, V. Monroche, P. Frère, P. Blanchard, P.J. Skabara, J. Roncali, Tetrahedron Lett., 44 (2003) 649-652.

[120] H. Brisset, S. Le Moustarder, P. Blanchard, B. Illien, A. Riou, J. Orduna, J. Garin, J. Roncali, J. Mater. Chem., 7 (1997) 2027-2032.

[121] E. Hadj Elandaloussi, P. Frère, P.F.A.d.e.R.J. Roncali, A.d.e. Riou, J. Roncali, New J. Chem., 22 (1998) 1051-1054.

[122] J.-f. Favard, P. Frère, A. Riou, A. Benahmed-gasmi, A. Gorgues, M. Jubault, J. Roncali, J. Mater. Chem., 8 (1998) 363-366.

[123] H. Brisset, C. Thobie-Gautier, M. Jubault, A. Gorgues, J. Roncali, J. Chem. Soc. Chem. Commun., (1994) 1765-1766.

[124] P. Frère, M. Allain, E.H. Elandaloussi, E. Levillain, F.-X. Sauvage, A. Riou, J. Roncali, Chem. Eur. J., 8 (2002) 784-792.

[125] Y. Yamashita, K. Ono, S. Tanaka, K. Imaeda, H. Inokuchi, Adv. Mater., 6 (1994) 295-298.

[126] M. Karikomi, C. Kitamura, S. Tanaka, Y. Yamashita, J. Am. Chem. Soc., 117 (1995) 6791-6792.

[127] G.C. Welch, R.C. Bakus, S.J. Teat, G.C. Bazan, J. Am. Chem. Soc., 135 (2013) 2298-2305.

[128] F. Di Maria, P. Olivelli, M. Gazzano, A. Zanelli, M. Biasiucci, G. Gigli, D. Gentili, P. D'Angelo, M. Cavallini, G. Barbarella, J. Am. Chem. Soc., 133 (2011) 8654-8661.

[129] F. Di Maria, M. Zangoli, M. Gazzano, E. Fabiano, D. Gentili, A. Zanelli, A. Fermi, G. Bergamini, D. Bonifazi, A. Perinot, M. Caironi, R. Mazzaro, V. Morandi, G. Gigli, A. Liscio, G. Barbarella, Adv. Funct. Mater., 28 (2018) 1801946.

[130] E. Salatelli, M. Marinelli, M. Lanzi, A. Zanelli, S. Dell'Elce, A. Liscio, M. Gazzano, F. Di Maria, J. Phys. Chem. C, 122 (2018) 4156-4164.

[131] R. Peng, H. Guo, J. Xiao, G. Wang, S. Tan, B. Zhao, X. Guo, Y. Li, ACS Appl. Energy Mater., 1 (2018) 2192-2199.